Jet dynamics and stability

Manel Perucho

Universitat de València

The innermost regions of relativistic jets and their magnetic fields

Granada, June 2013

Outline

- Spectral evolution of CTA 102.
  - Possible evidence for shock-shock interaction in the core region:
    - Fromm et al. 2011, 2012, Fromm et al. (submitted), Fromm et al. (in preparation).

- Helical patterns in 0836+710.
  - Detection of wave motion:
    - Perucho et al. 2012a,b.

CTA 102 – light curve

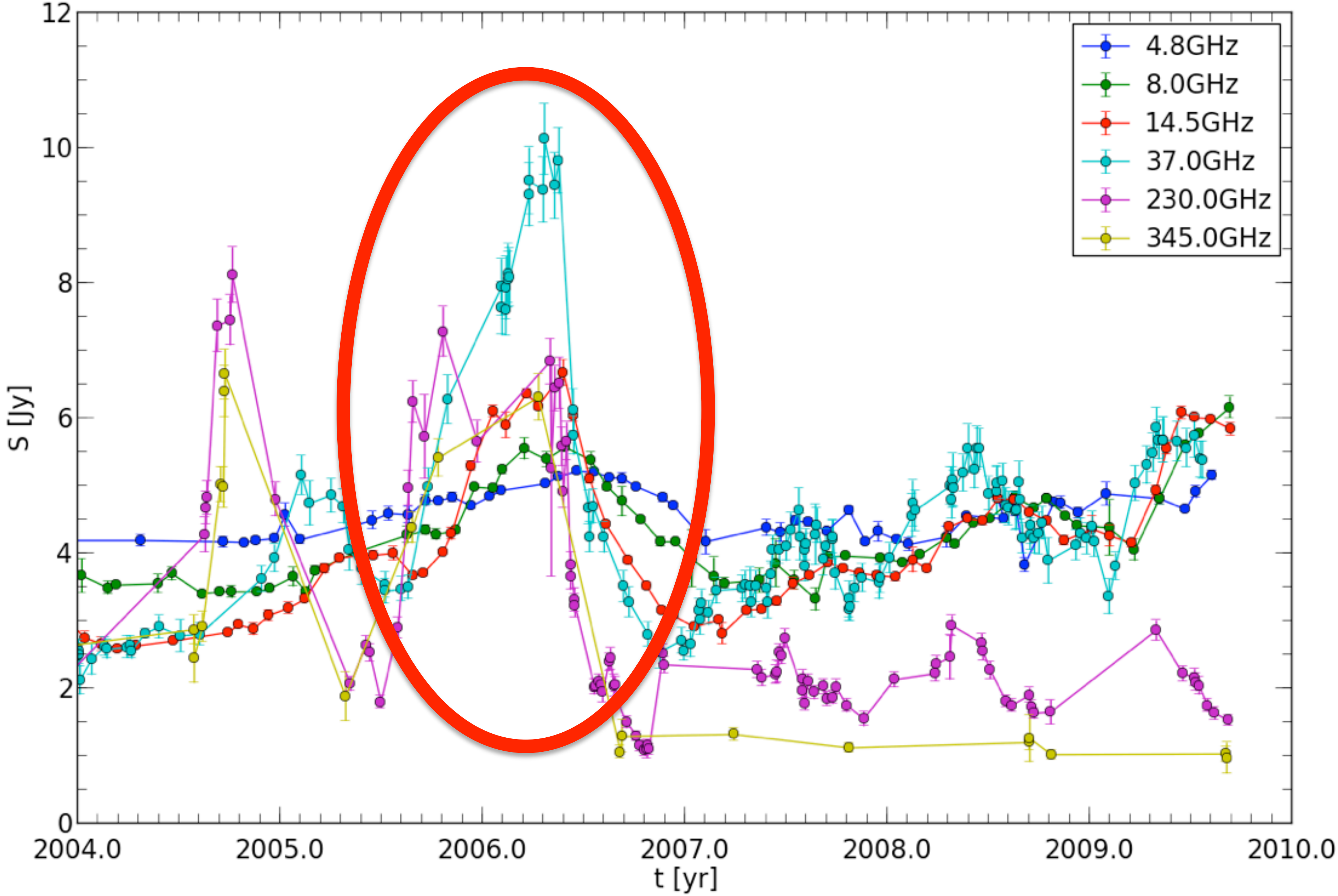

Fromm, MP, Ros, et al. 2011

CTA 102 – spectrum

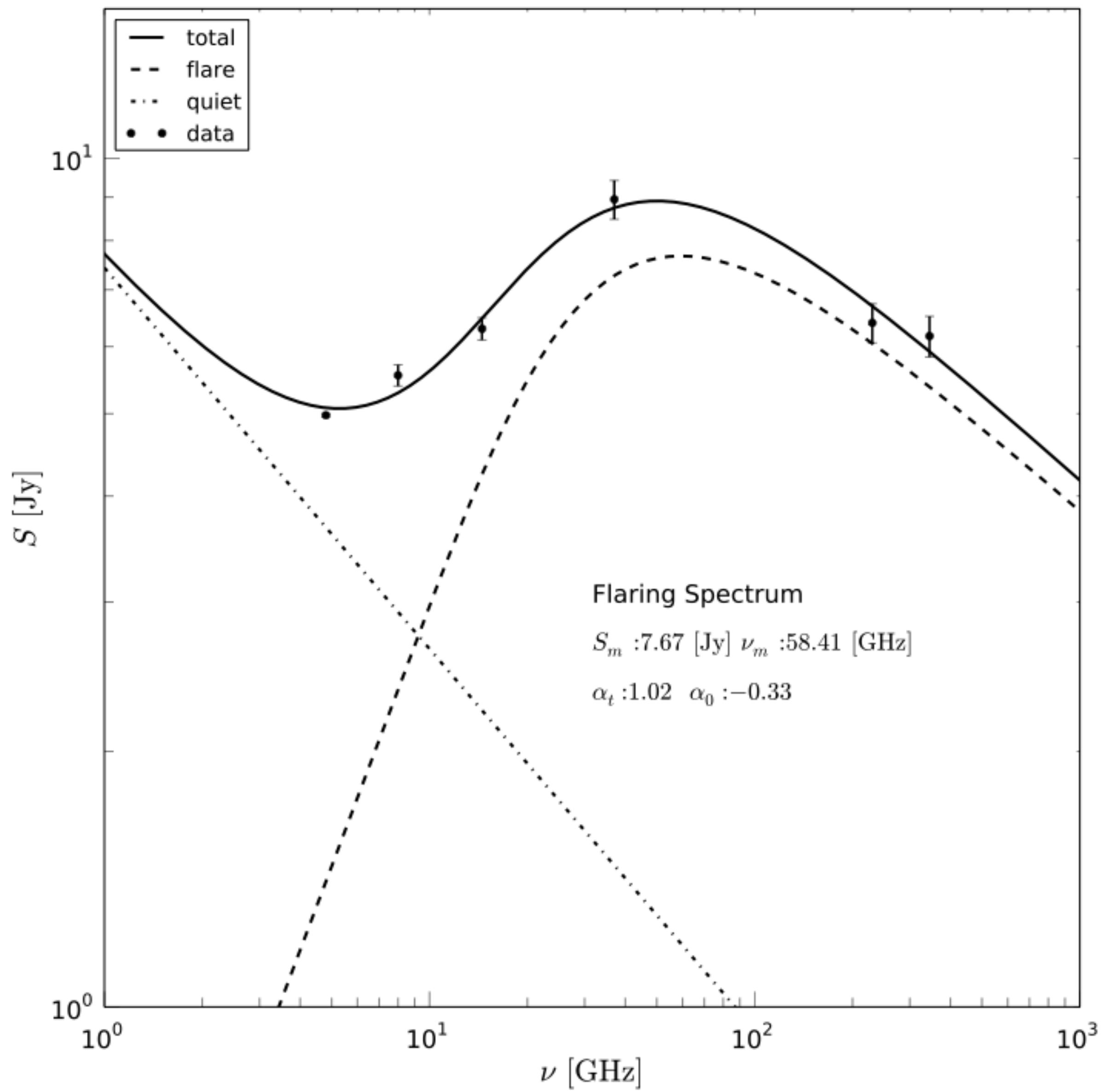

Computing a "steady state" spectrum, the flaring part can be isolated.

And derived for each observation.

Fromm, MP, Ros, et al. 2011

CTA 102 – spectral evolution of the flare

conical jet

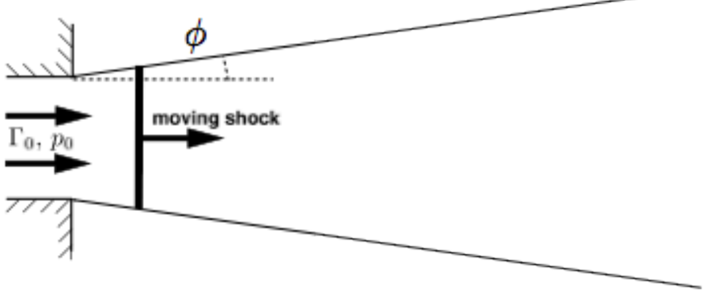

A simple trial to fit the spectral evolution of the flare within the three stages of cooling within the shock-in-jet-model (Marscher and Gear 1985): Compton, Synchrotron and Adiabatic.

It fails to explain the double peak.

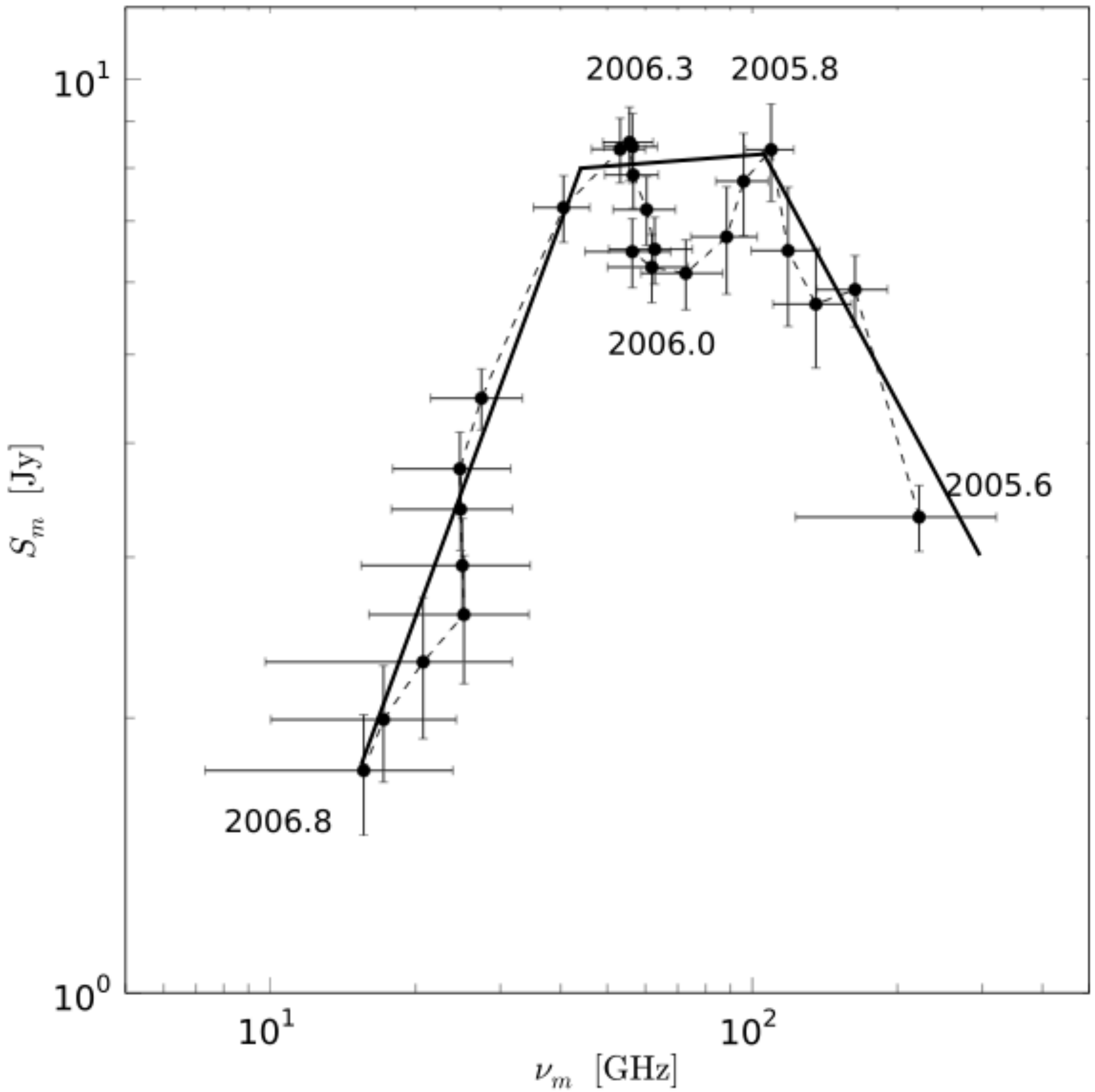

Fromm, MP, Ros, et al. 2011

CTA 102 – spectral evolution of the flare

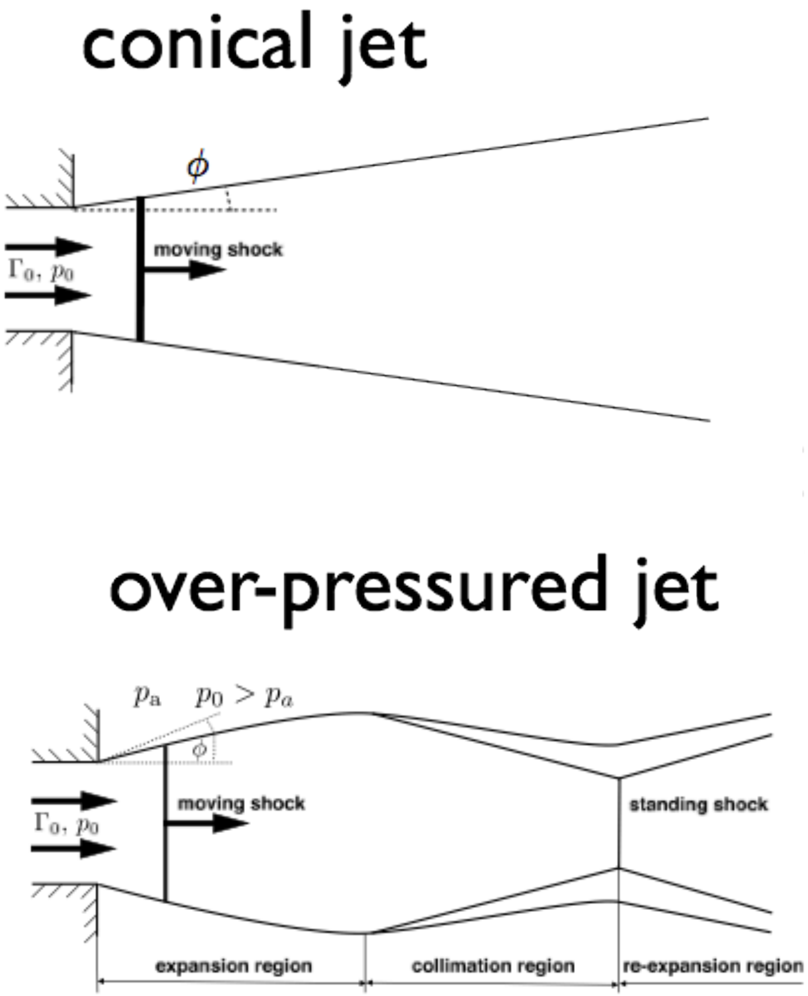

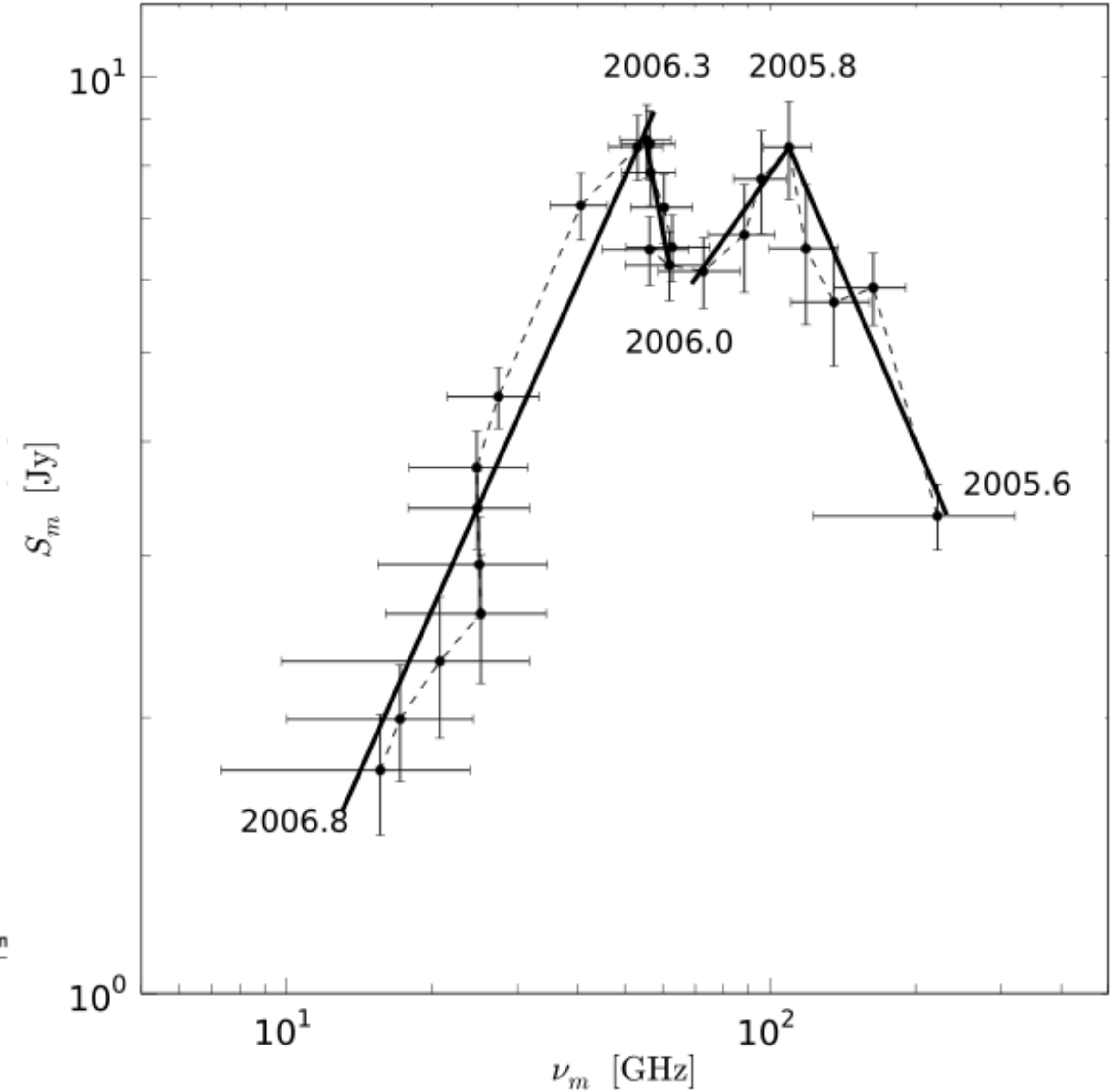

Fromm, MP, Ros, et al. 2011

CTA 102 – VLBI observations

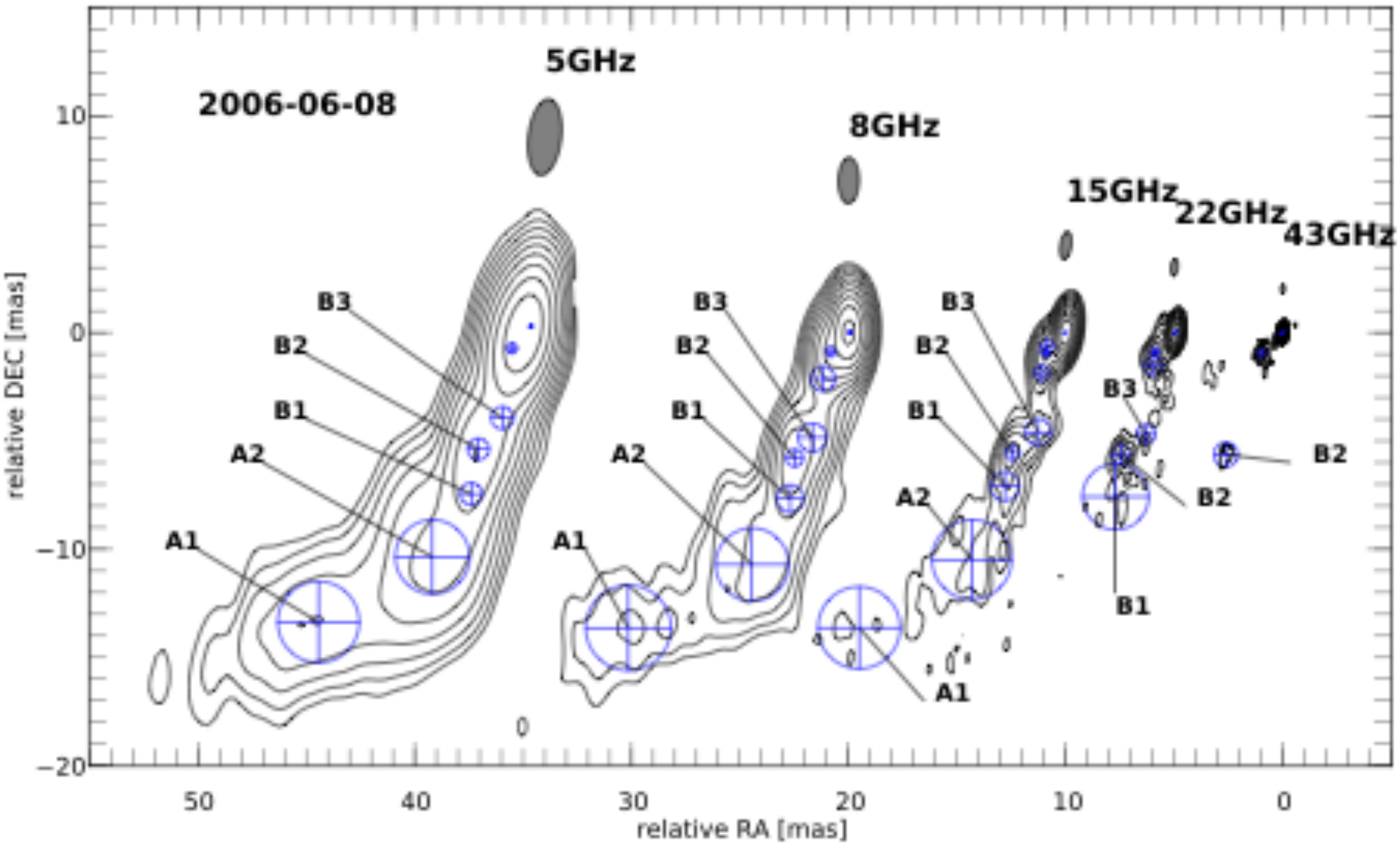

Fromm, Ros, MP, et al. 2012, MOJAVE (Lister et al. 2009)

CTA 102 – kinematics

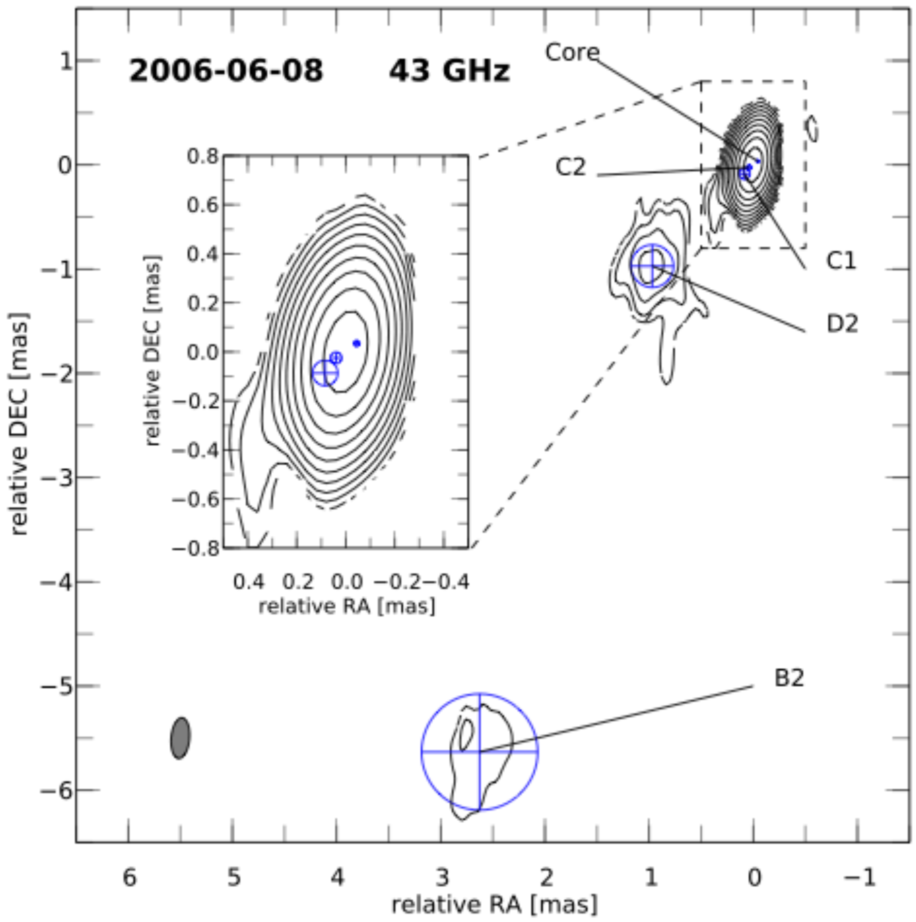

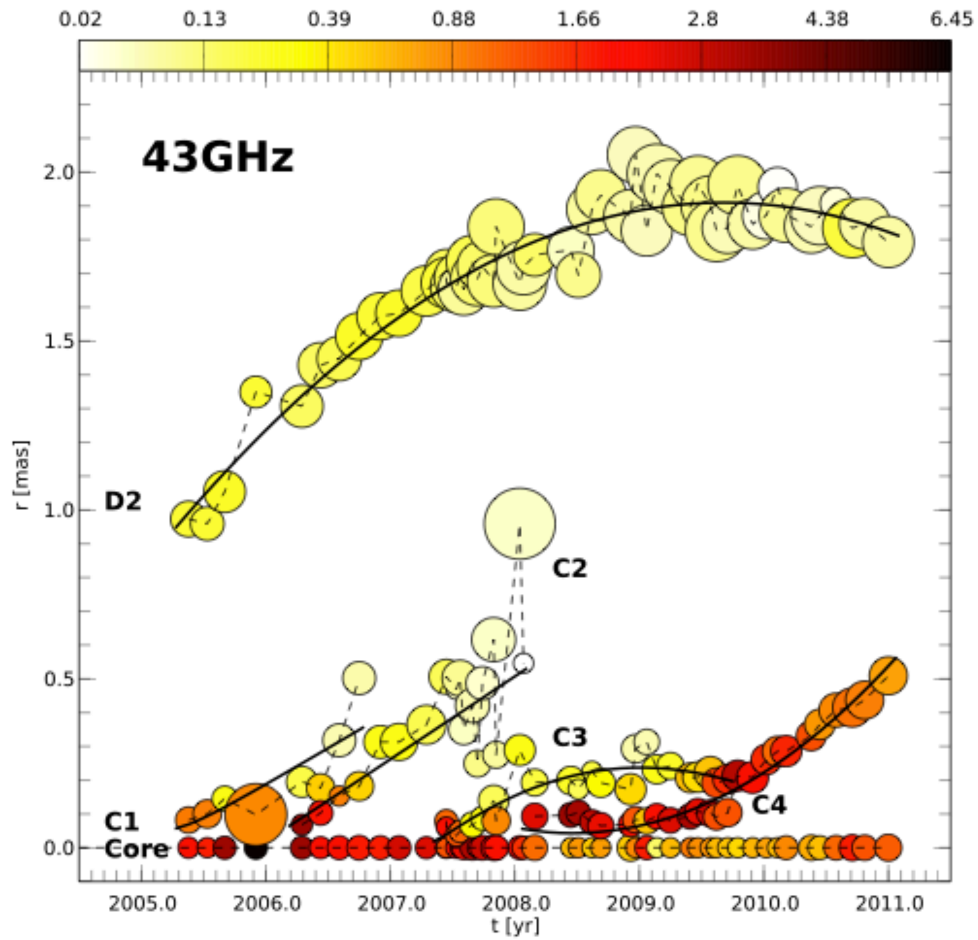

Fromm, Ros, MP, et al. 2012

CTA 102 – kinematics

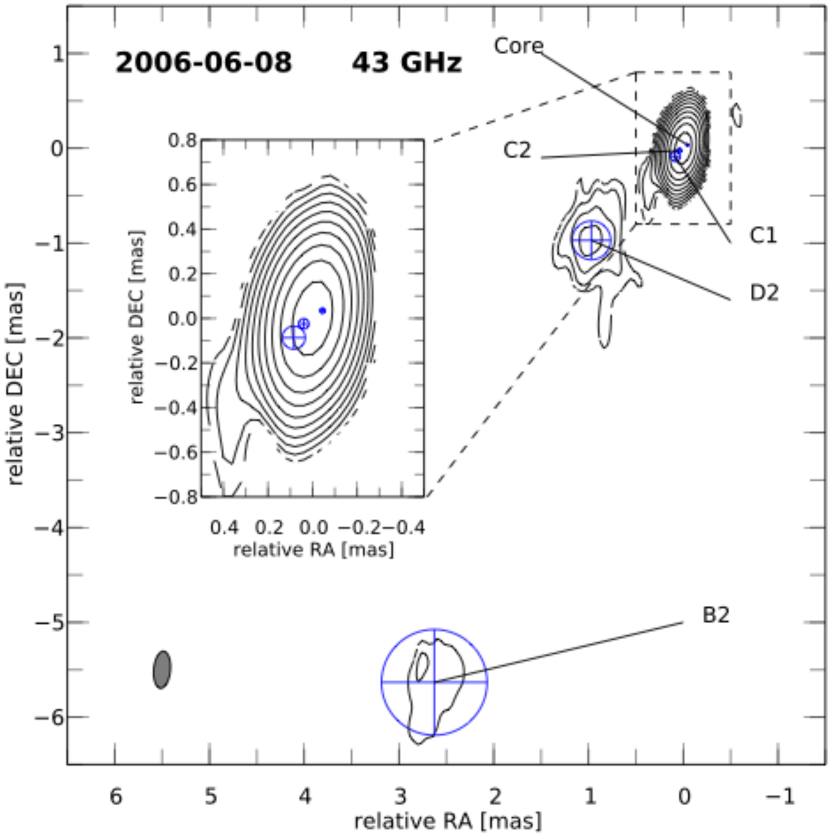

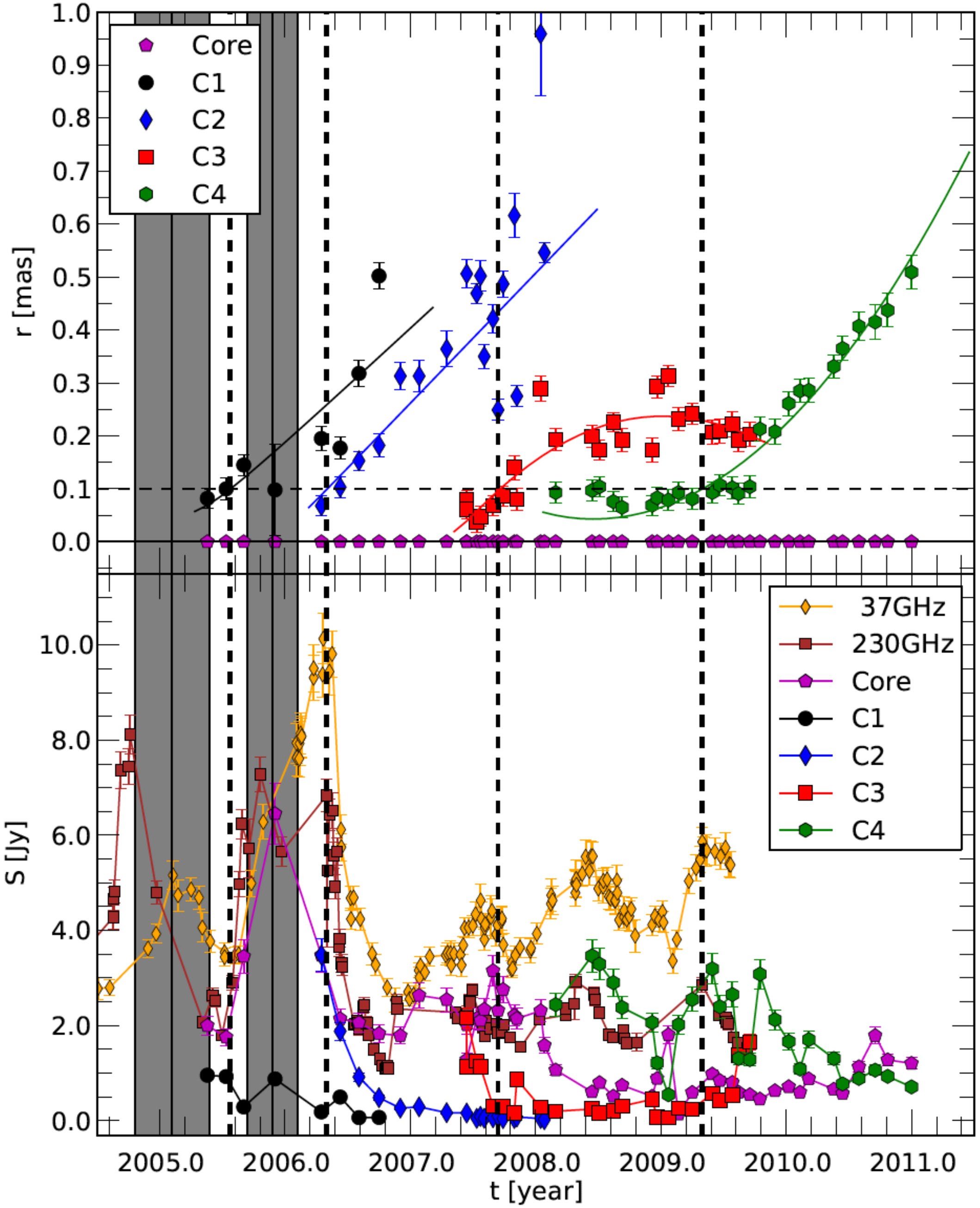

Fromm, Ros, MP, et al. 2012

CTA 102 – kinematics and spectral analysis

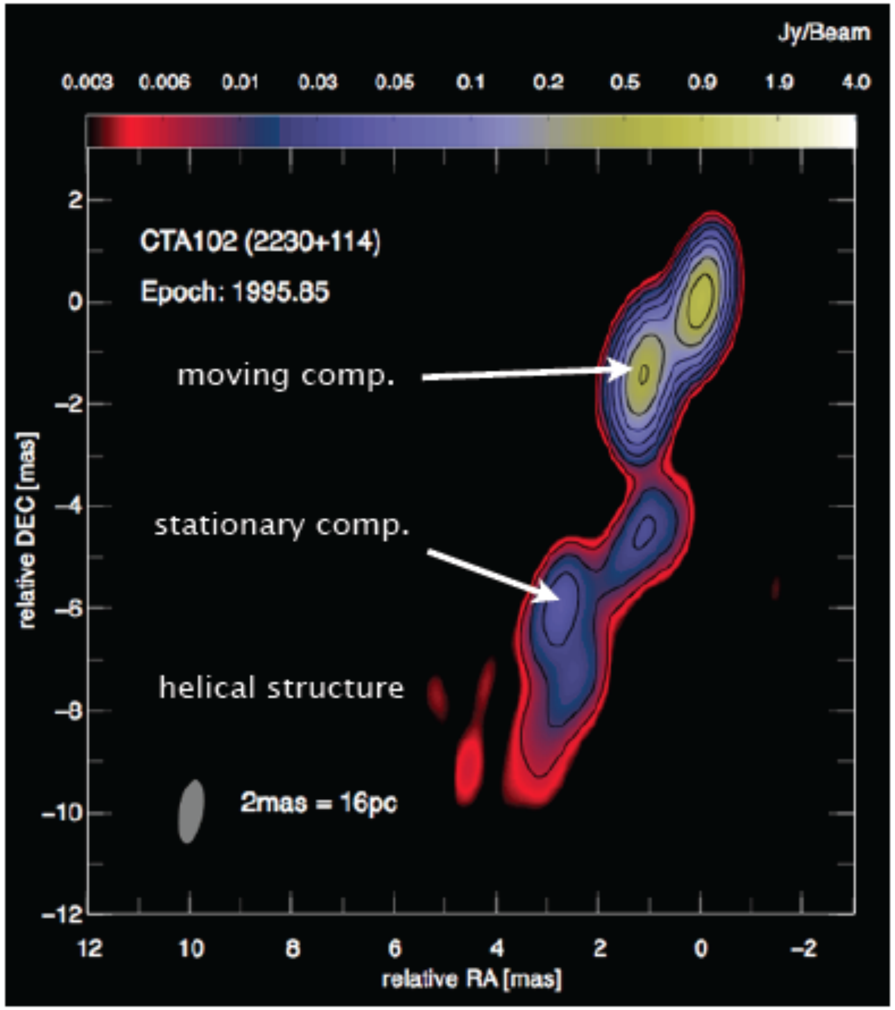

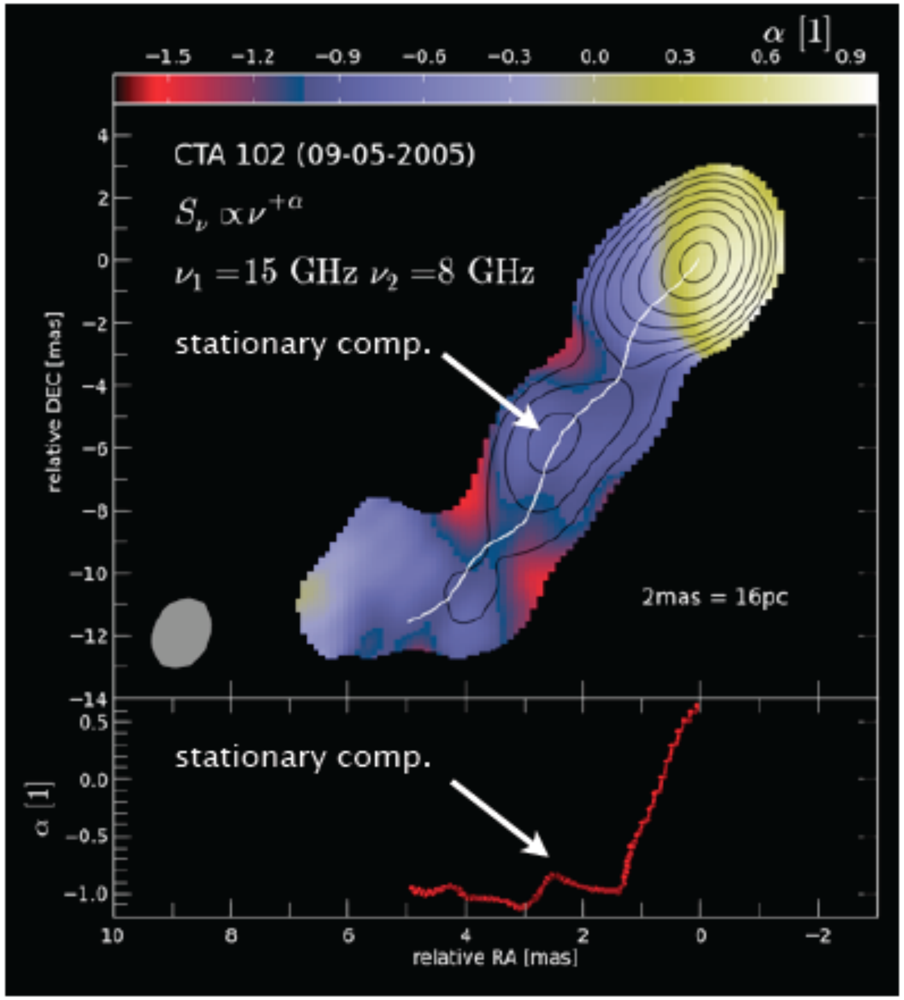

Unfortunately, the resolution in the region of interest (~ 0.1 mas) is not enough to study our hypothesis in detail. However…

Fromm, Ros, MP, et al. 2011, Fromm, Ros, MP, et al., submitted

CTA 102 – hints of standing shocks

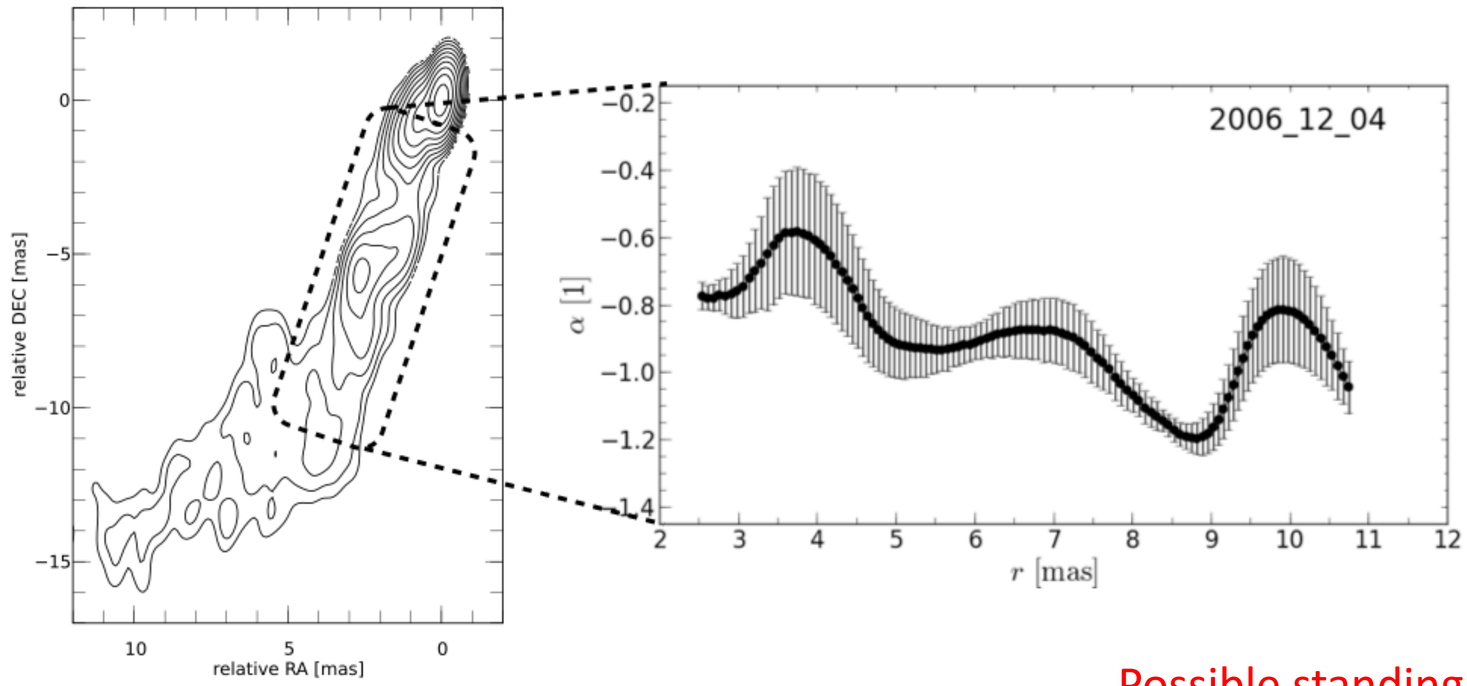

Spectral index in a region with small errors.

Fromm, Ros, MP, et al., submitted

Possible standing shocks at 3-10 mas

Mimica et al. 2009

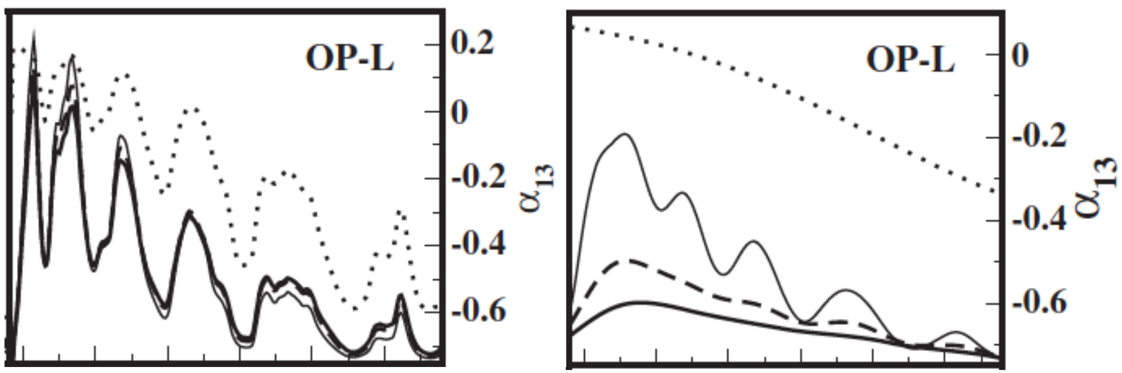

Spectral index from a simulation of an over-pressured jet (without and with convolution).
Reconfinement shocks are indicated by increases in flux and spectral index (if enough resolution).

CTA 102 – numerical experiment

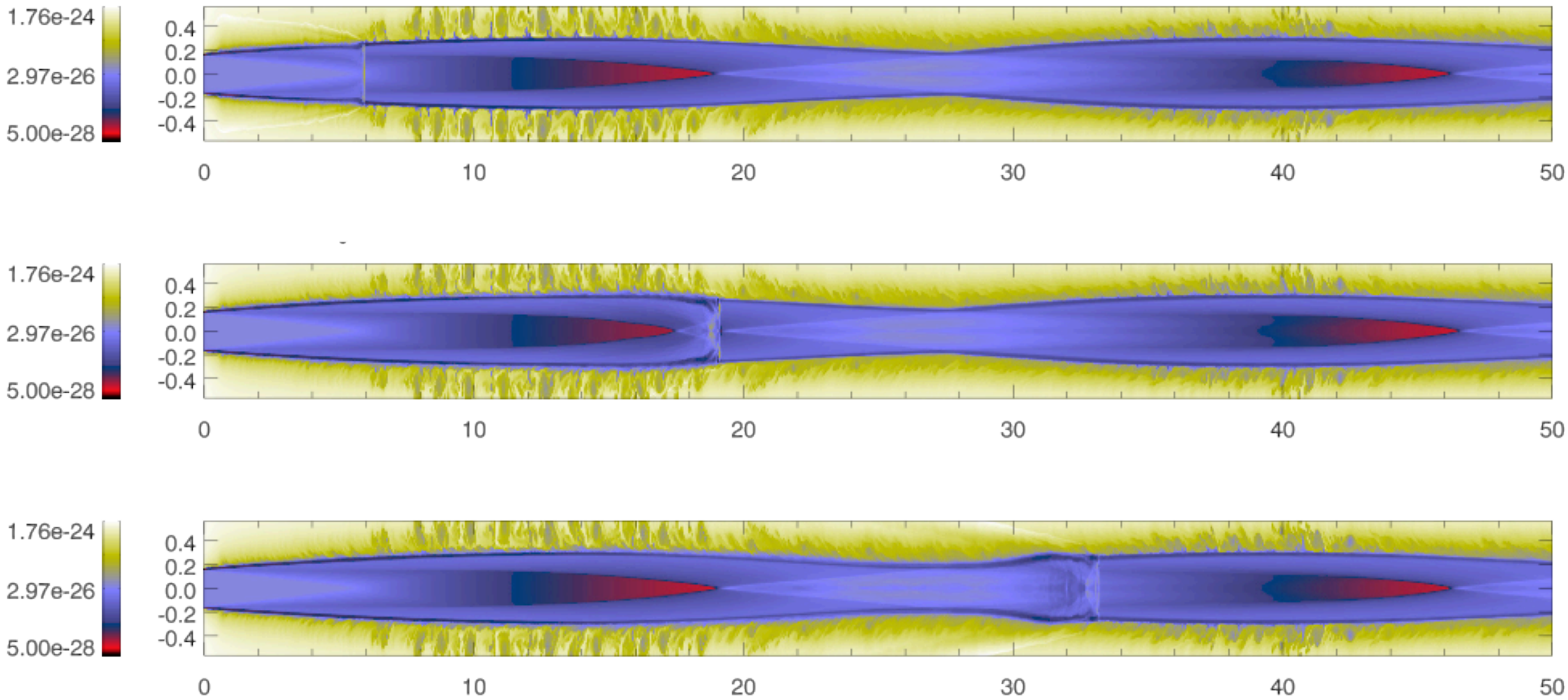

Numerical simulation of the evolution of a perturbation propagating through an overpressured jet

- performed at Tirant, node of the Spanish Supercomputational Network at the University of València.

Fromm, MP, et al., in preparation

CTA 102 – numerical experiment:
emission and spectrum

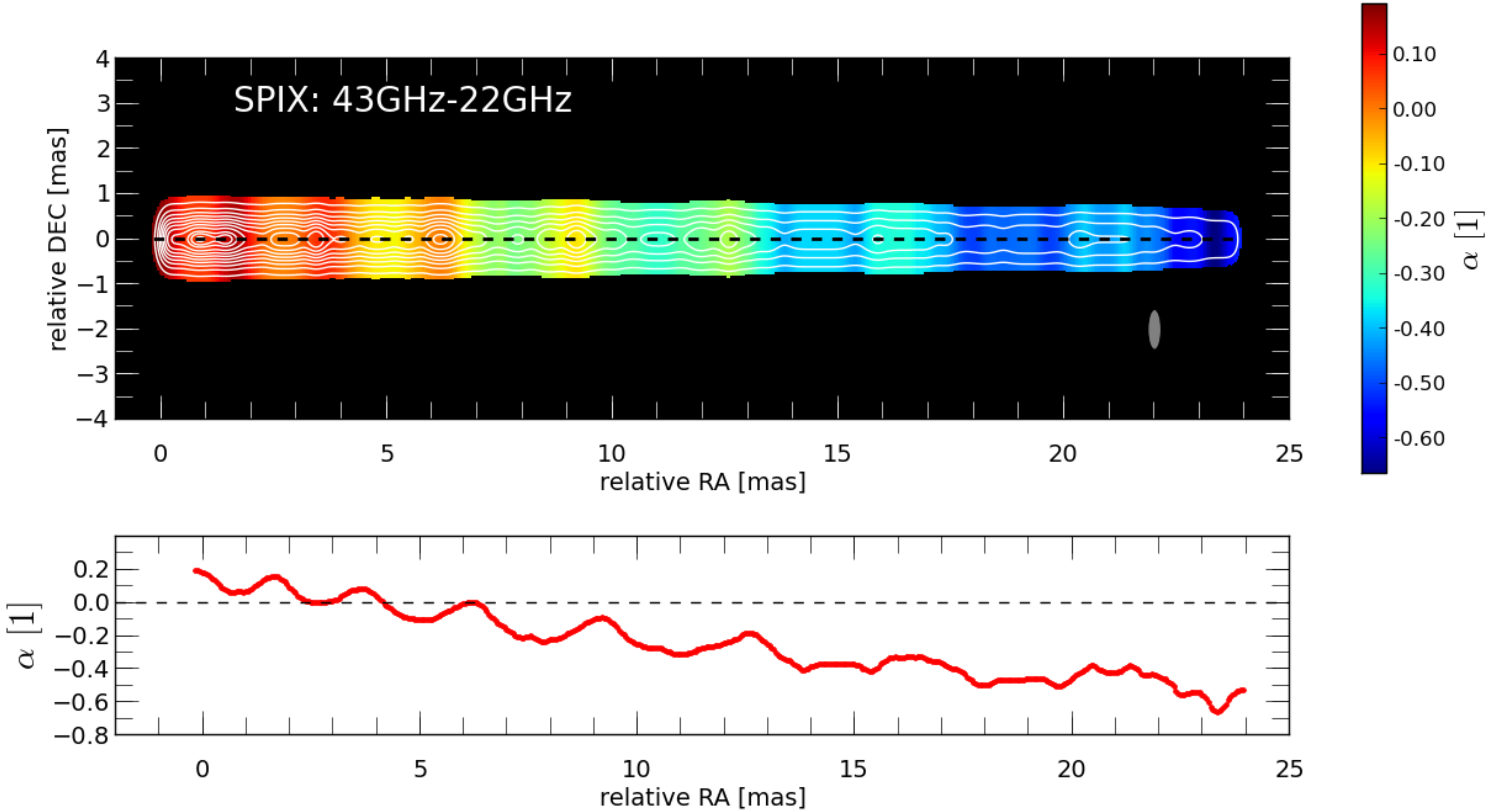

The emission is computed at 90º viewing angle. The standing shocks also show bumps in the spectral index.

Gómez et al. 1997, Mimica et al. 2009, Fromm, MP, et al., in preparation

CTA 102 – numerical experiment:
kinematics

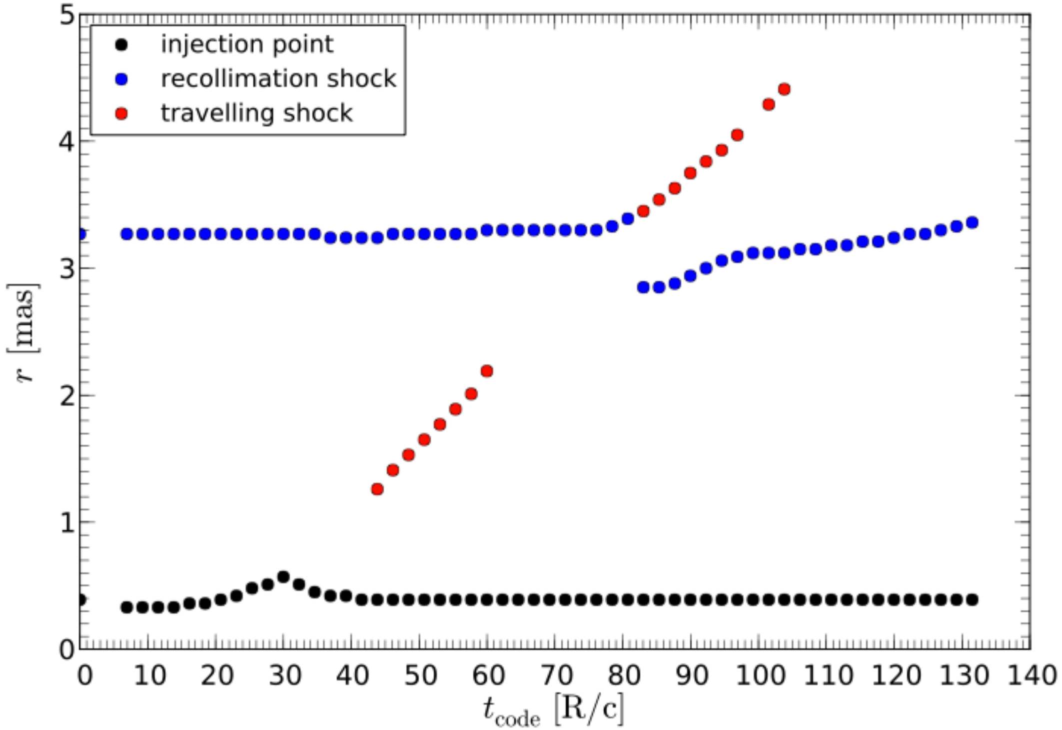

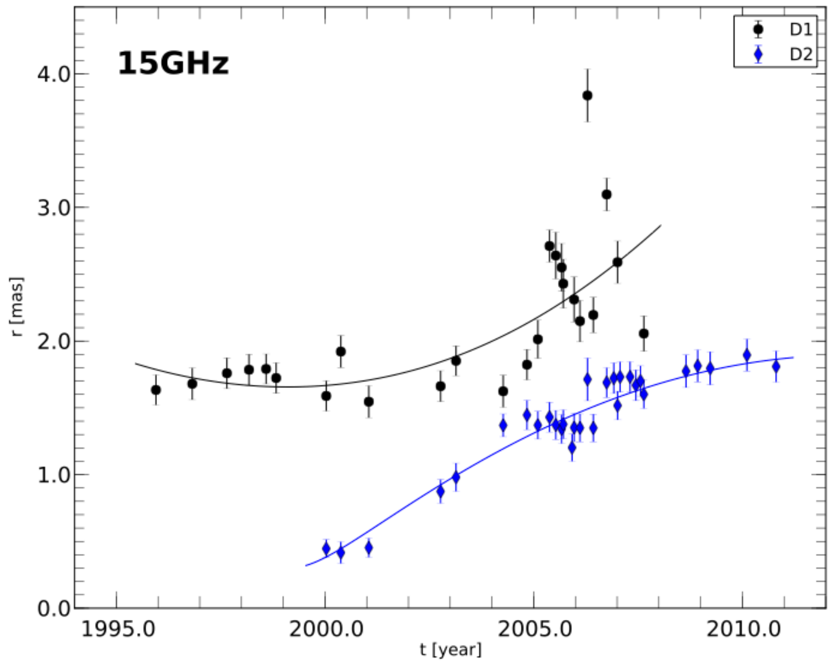

Fitting Gaussian components to the simulated jet, we are able to track the interaction between the standing shock and the perturbation.

We can then revisit this identifi-cation of components at 2 mas, which is a region closer to the nucleus than the one shown for the spectral index.

CTA 102 – numerical experiment:
kinematics

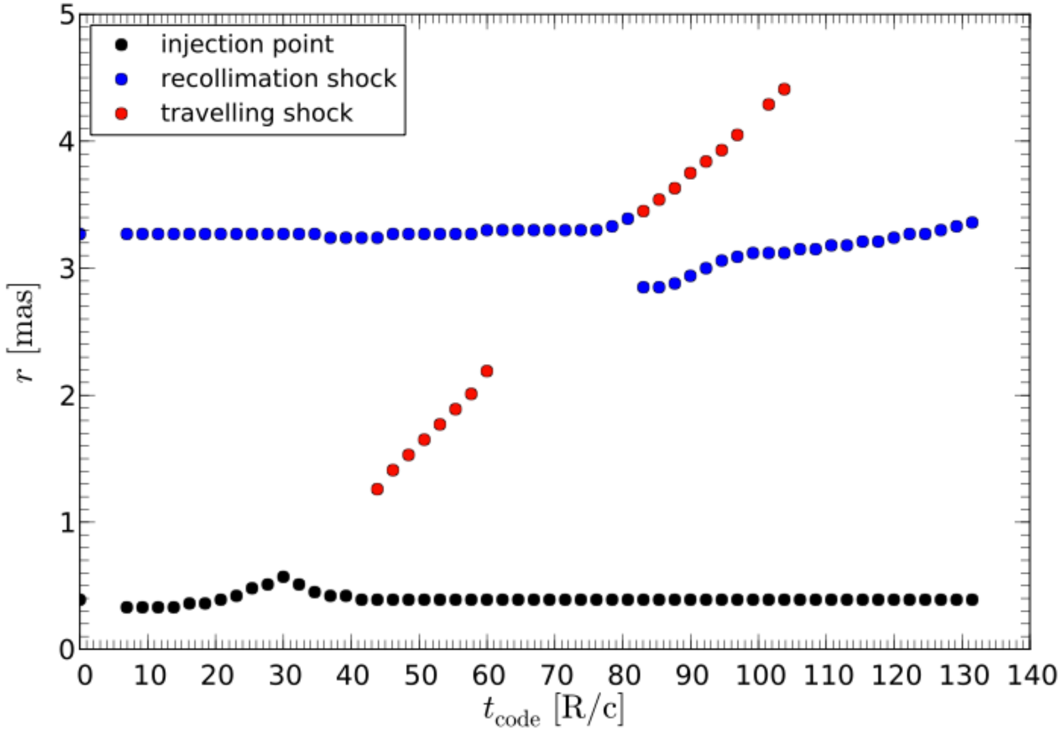

Fitting Gaussian components to the simulated jet, we are able to track the interaction between the standing shock and the perturbation.

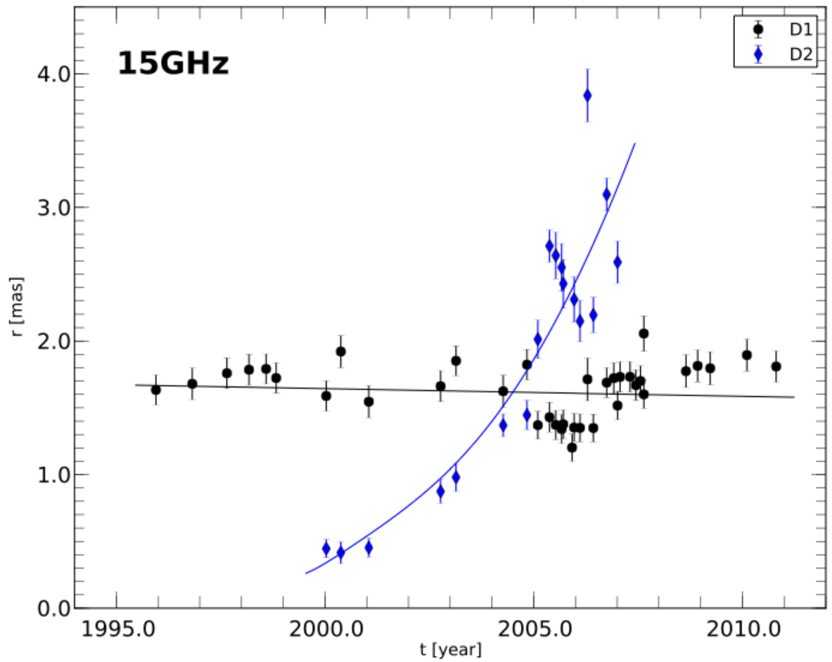

We can then revisit this identifi-cation of components at 2 mas, which is a region closer to the nucleus than the one shown for the spectral index:

Possible shock-shock interaction at 2 mas…

Perturbation associated to a previous flare (late nineties).

CTA 102 – numerical experiment: spectral evolution

Peak flux of the flaring spectrum from the simulation

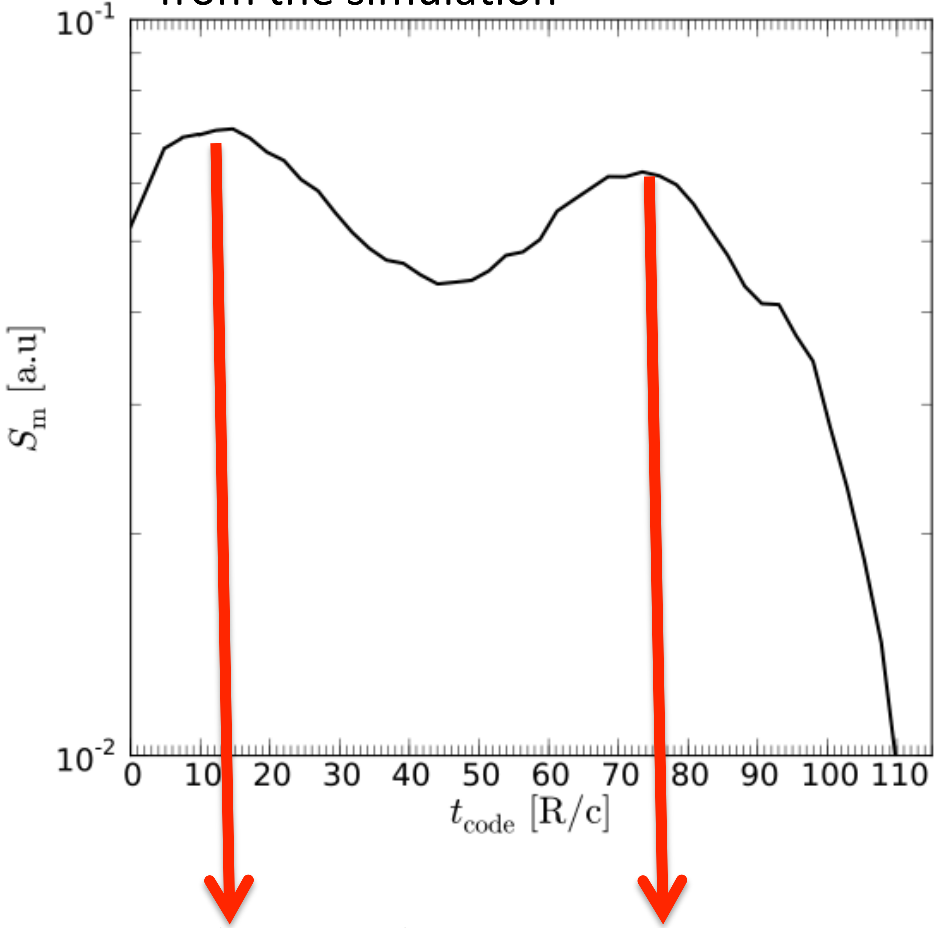

first peak (injection)

Second peak: crossing of the recollimation shock.

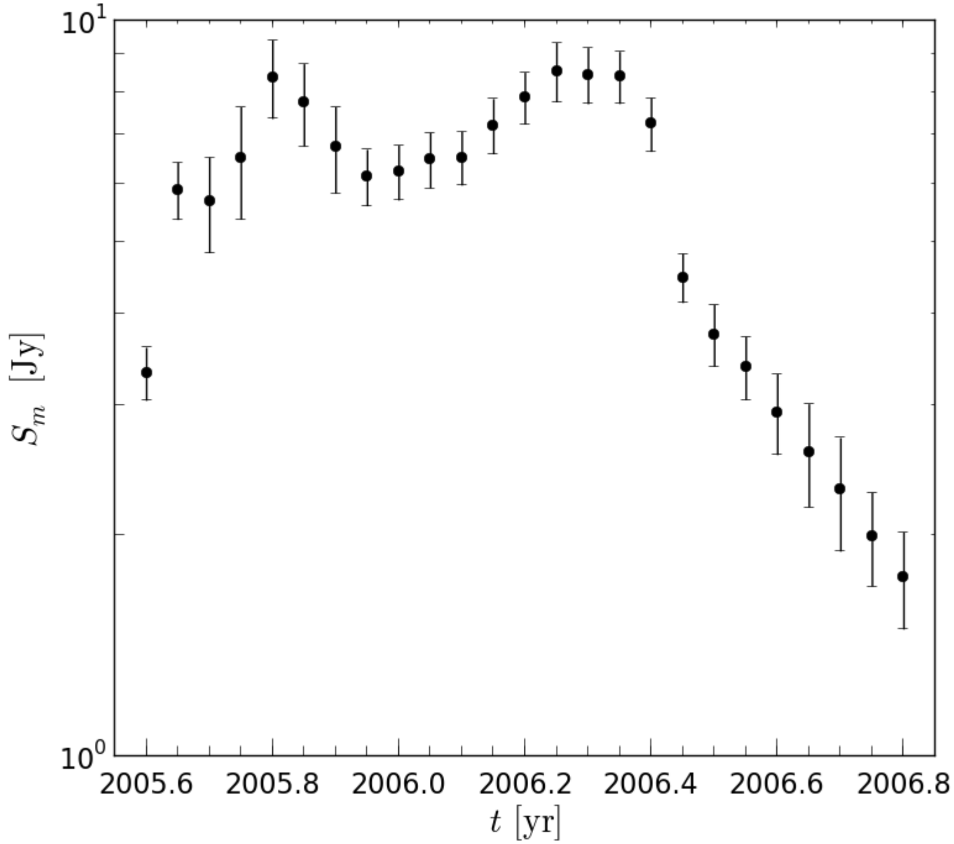

Observed evolution of the flaring spectrum in CTA102.

Conclusions

- Light curve + VLBI kinematics + spectral analysis + numerical simulations.
  - Evidence, from spectral analysis, for standing shocks at the 3-10 mas region.
  - Evidence, from numerical simulations, compared with the observations, of:
    - Shock-shock interaction at ~ 2 mas.
    - Shock-shock interaction at ~ 0.1 mas.
      - NOTE: This is within the core region with our current resolution, but it is not the core itself.

S5 0836+710

The large-scale structure of the jet is diffuse and irregular, with no trace of a hotspot.

Quasar, z=2.16. Classified as an FRII in terms of luminosity (O'Dea et al. 1988).

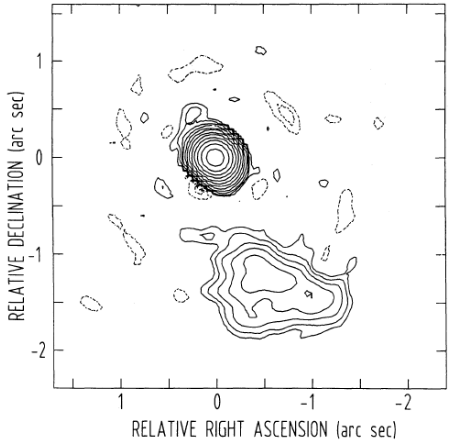

MERLIN – 1.6 GHz

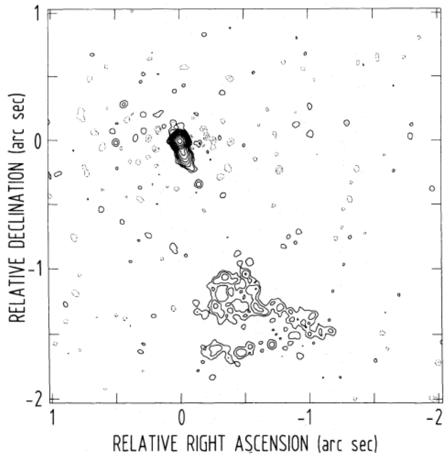

EVN-MERLIN – 1.6 GHz

Krichbaum et al. 1990,
Hummel et al. 1992

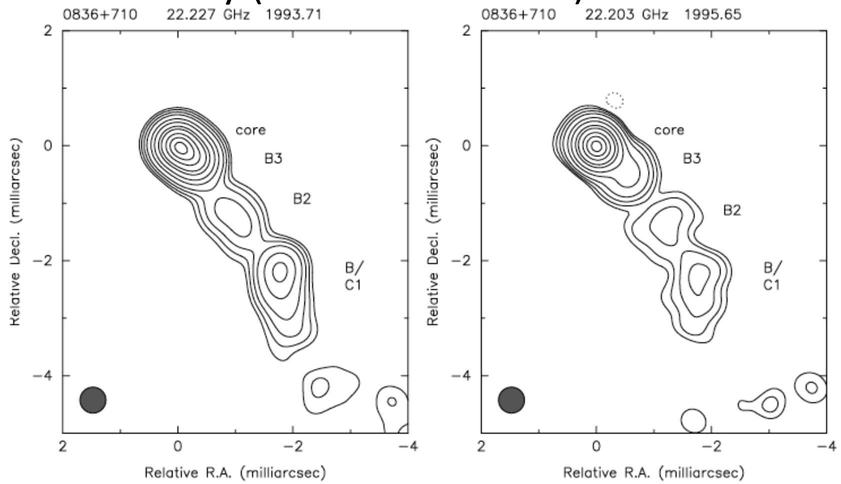

G-VLBI – 22 GHz

Otterbein et al. 1998

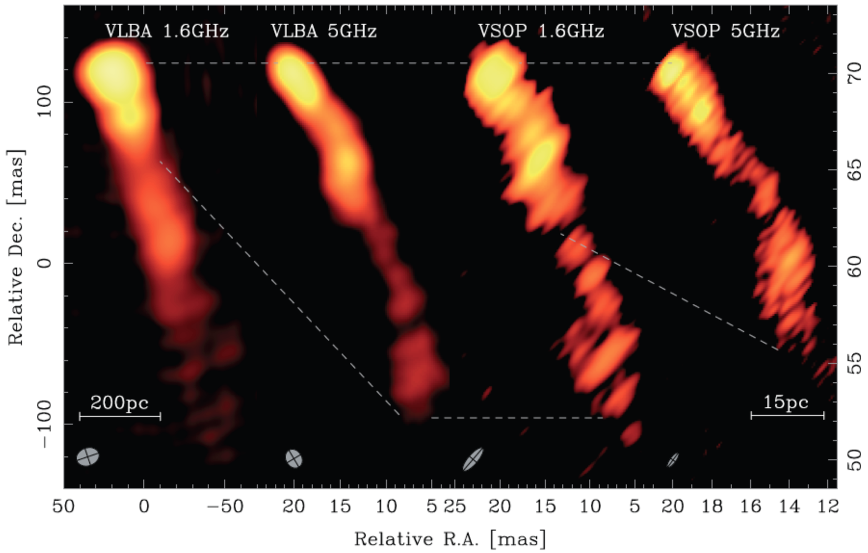

VLBA – VSOP
1.6 – 5 GHz
Lobanov et al. 2006

1 mas = 8.4 pc
Viewing angle = 3º

Observations of S5 0836+710

We have used different observations of the jet in the quasar 0836+710.

YEAR	1.6 GHz	2 GHz	5 GHz	8 GHz	15 GHz	22 GHz	43 GHz
1997	VLBA	G-VLBI	VLBA	G-VLBI	...	...	...
1998	VLBA	...	...	VLBA	VLBA	VLBA	VLBA
1999	...	...	...	VLBA	VLBA	VLBA	VLBA
2000	...	...	...	...	VLBA	...	...
2001	...	...	...	...	VLBA	...	...
2002	...	...	...	...	VLBA	...	...
2003	VLBA	...	VLBA	...	VLBA	VLBA	VLBA
2004	...	...	...	...	VLBA	...	...
2005	...	...	...	...	VLBA	...	...
2006	...	...	...	...	VLBA	...	...
2007	EVN	...	...	...	VLBA	...	...
2008	EVN	...	...	...	VLBA	...	...
2009	...	...	...	...	VLBA	...	...

Perucho, Kovalev, Lobanov, Hardee & Agudo 2012, ApJ, 749, 55

Lobanov et al. 2006
Pushkarev & Kovalev 2011
MOJAVE database
(Lister et al. 2009)
Perucho et al. 2012

Ridge-lines

We define the ridge-line as the peak of the Gaussian fitted to the jet profile at each radial distance from the core.

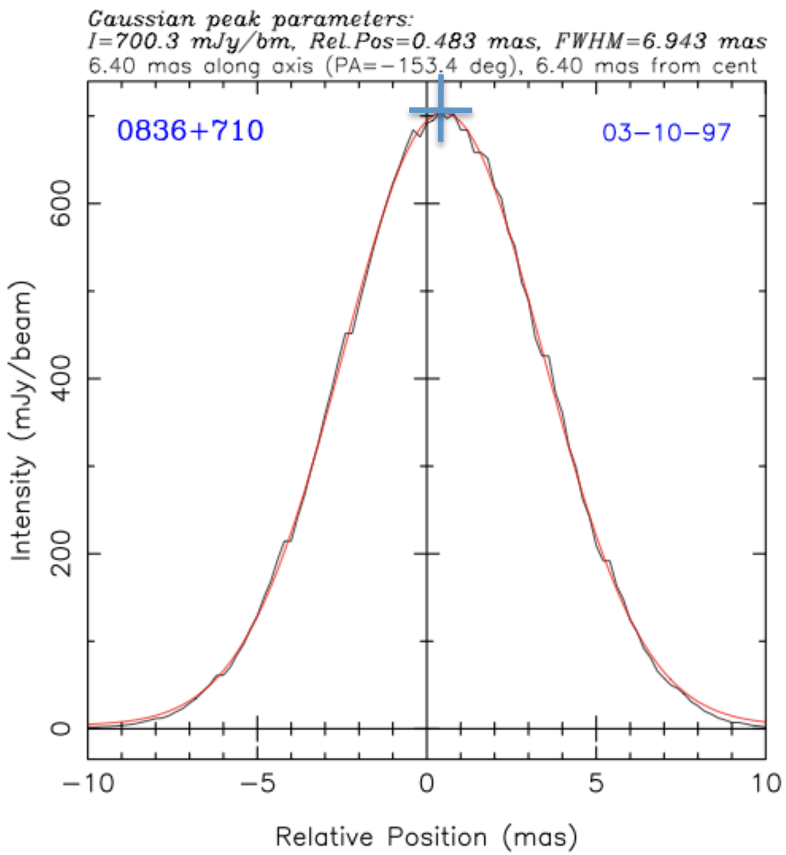

1.6 GHz

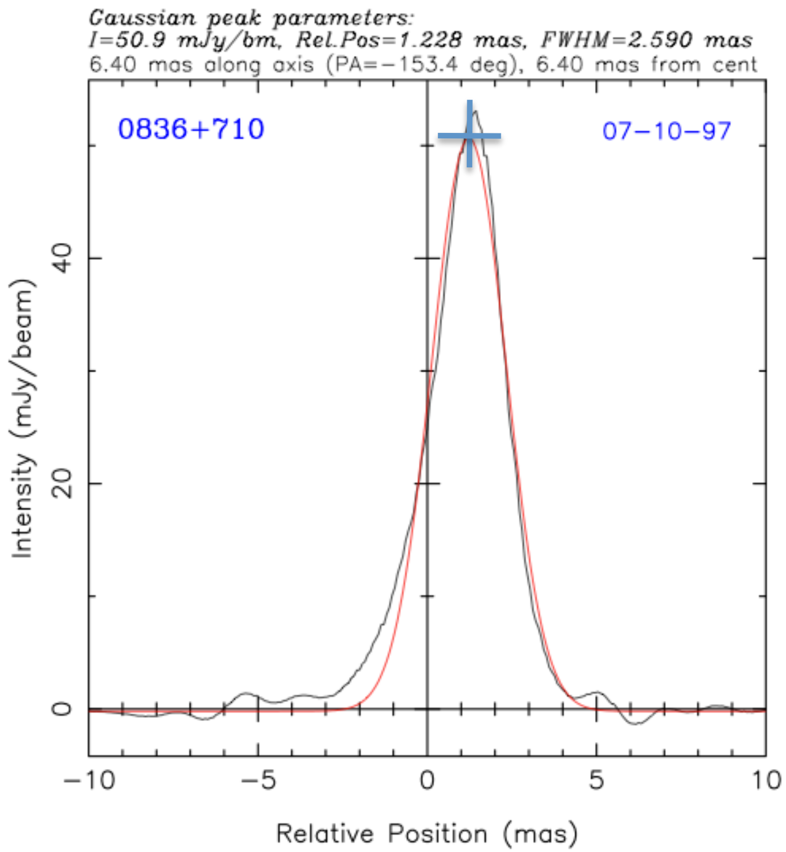

8 GHz

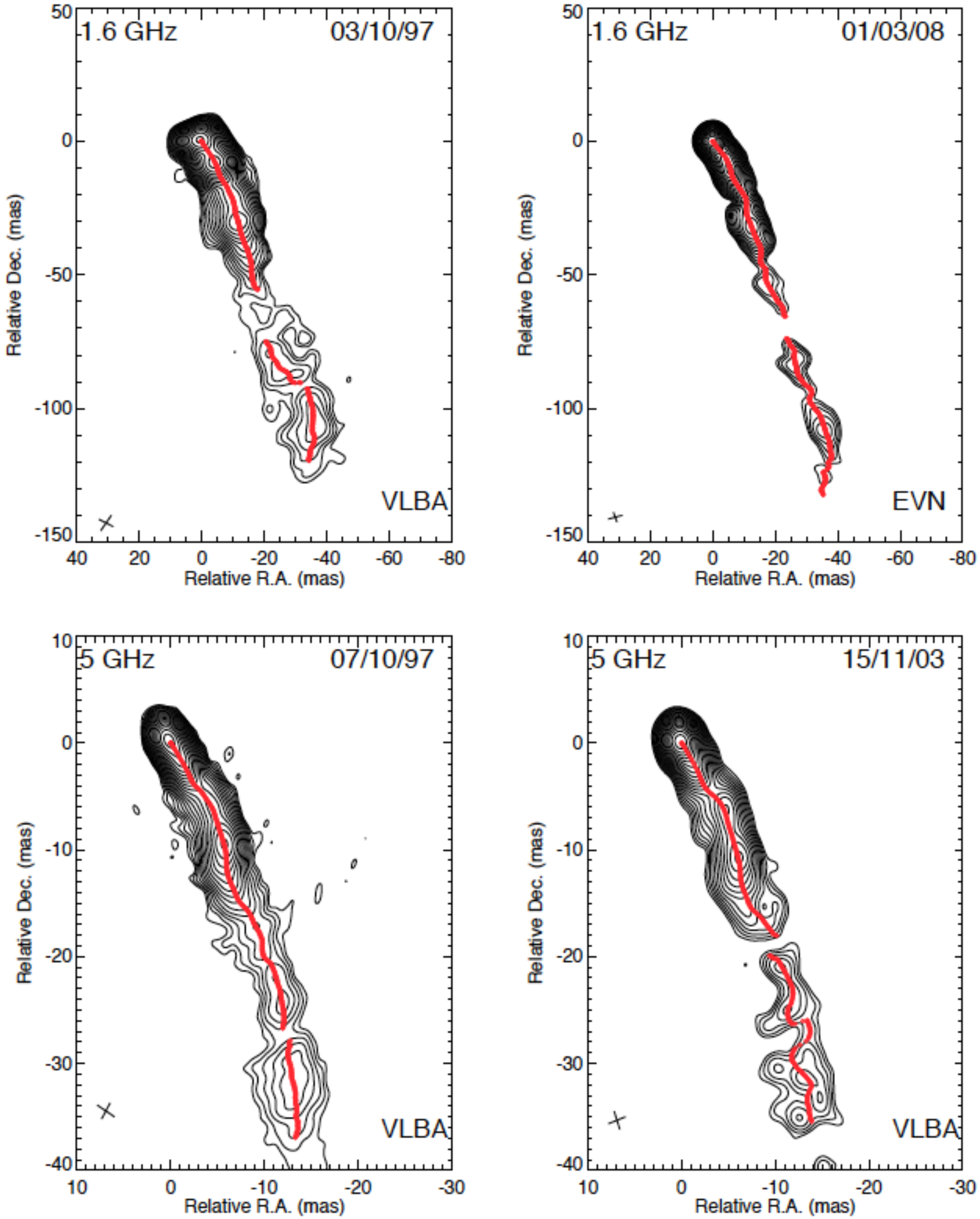

Ridge-lines

The ridge-line points indicate the
peak of a Gaussian fitted to
the jet profile at each
radial distance from the core.

Ridge-lines at different frequencies

The ridge-lines obtained at different frequencies coincide within errors

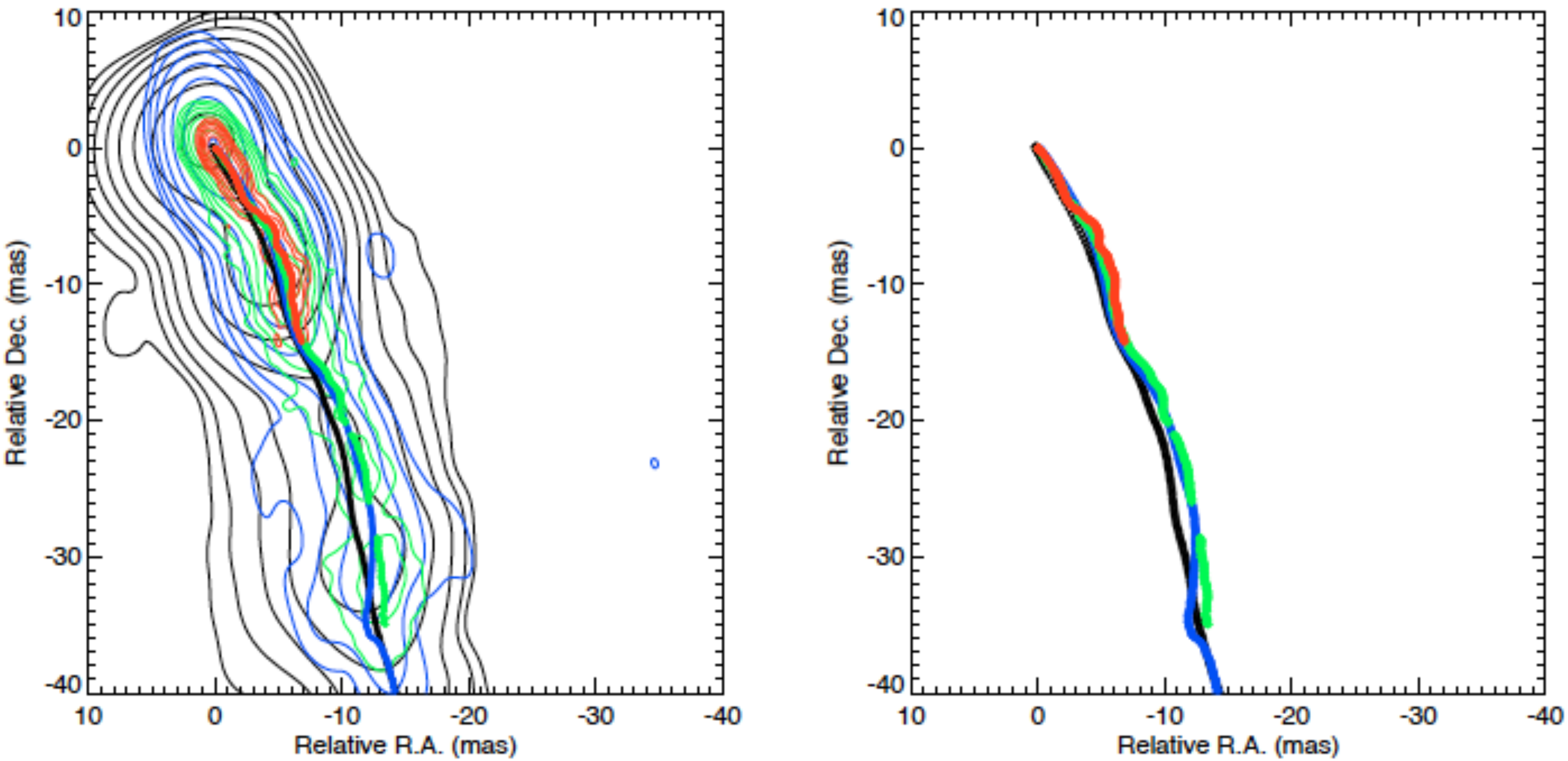

1.6 (black), 2 (blue), 5 (green) and 8 (red) GHz (1997)

Ridge-lines at different frequencies

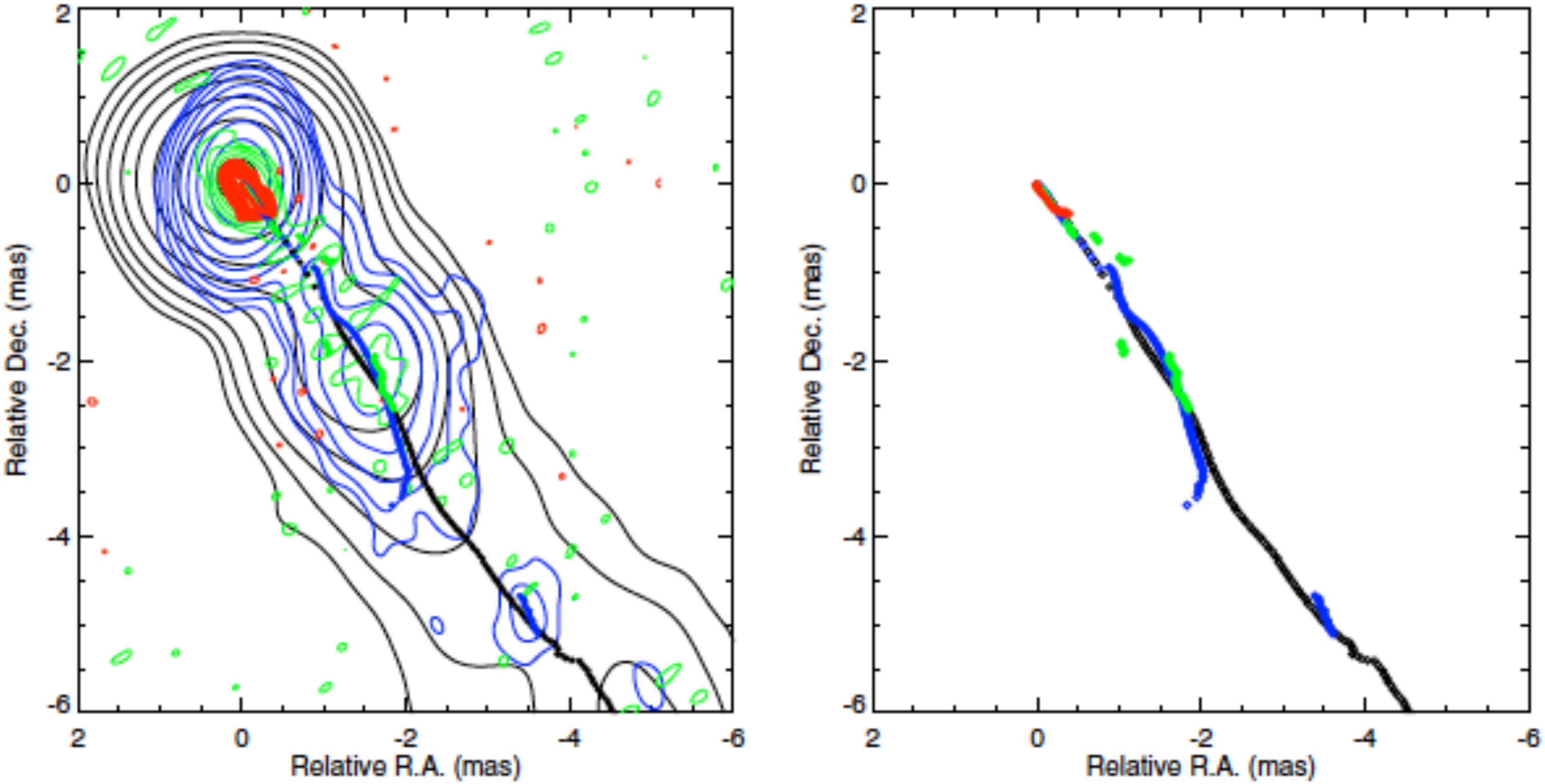

8 (black), 15 (blue), 22 (green) and 43 (red) GHz (1998)

Defining an axis

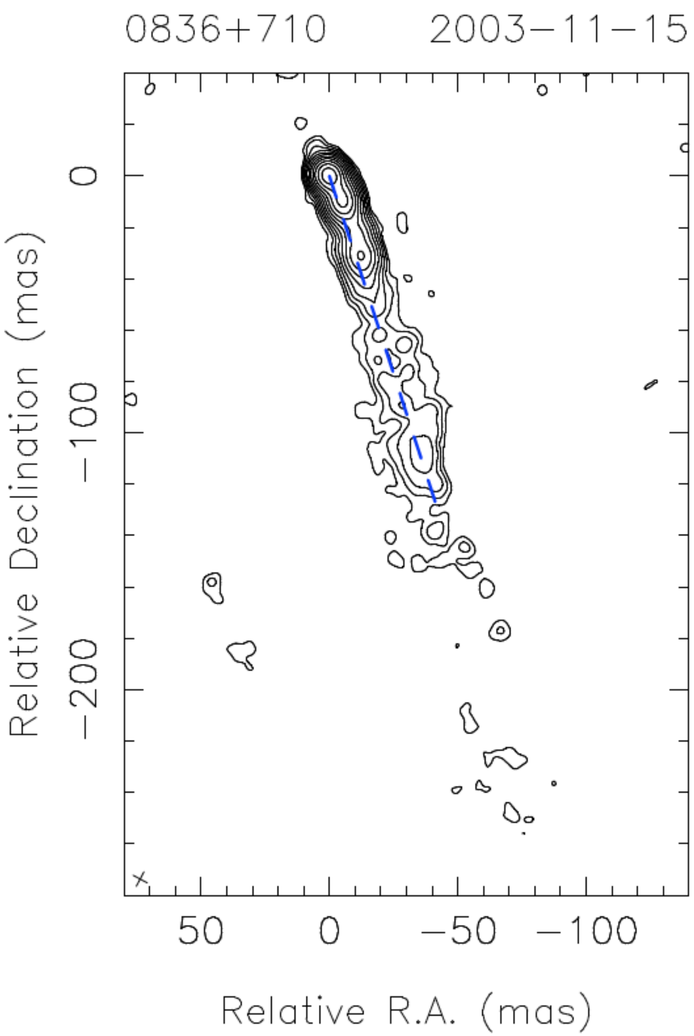

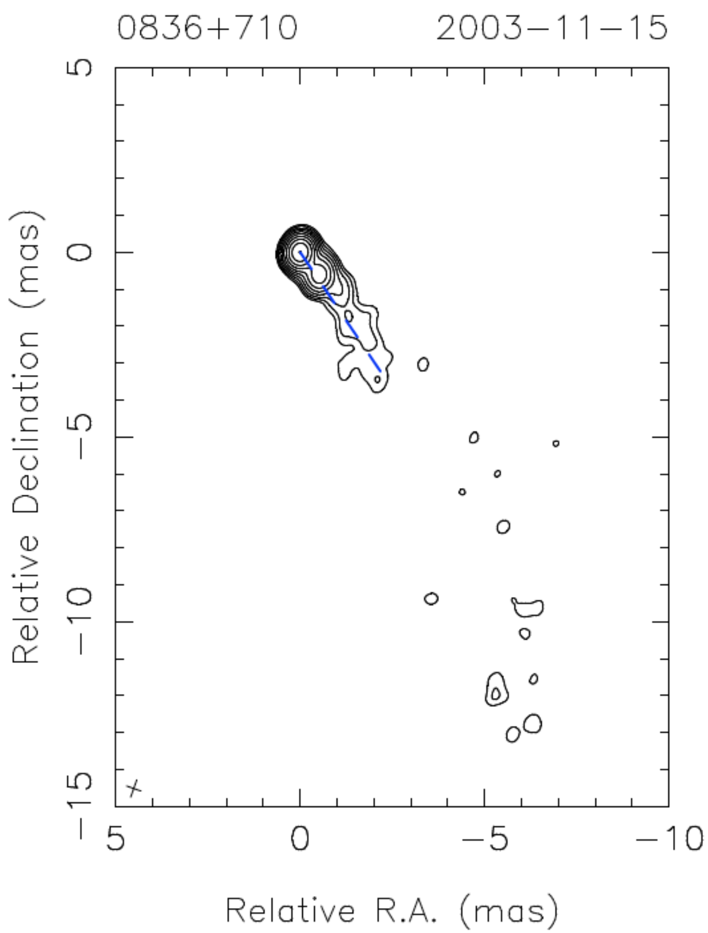

We determined the position angle of the jet at each frequency by connecting the core with the emission at the largest observed distances (it can also be done by making the oscillations symmetric around this axis).

Observed opening angles and position angles

Table 2. Observed Jet properties.

	1.6 GHz	5 GHz	8 GHz	15 GHz	22 GHz	43 GHz
Average opening angle	$(12.3 \pm 1.2)^\circ$	$(13.5 \pm 1.3)^\circ$	$(12.1 \pm 0.8)^\circ$	$(10.5 \pm 0.9)^\circ$	18.1°	16.6°
Position angle (χ)	198°	202°	206°	210°	214°	-
Oscillation wavelengths (0-10 mas)	10 - 80	10	10	10	-	-
Oscillation wavelengths (10-35 mas)	20 - 80	20	7-20	20	-	-
Oscillation wavelengths (>35 mas)	40 - 80	-	-	-	-	-

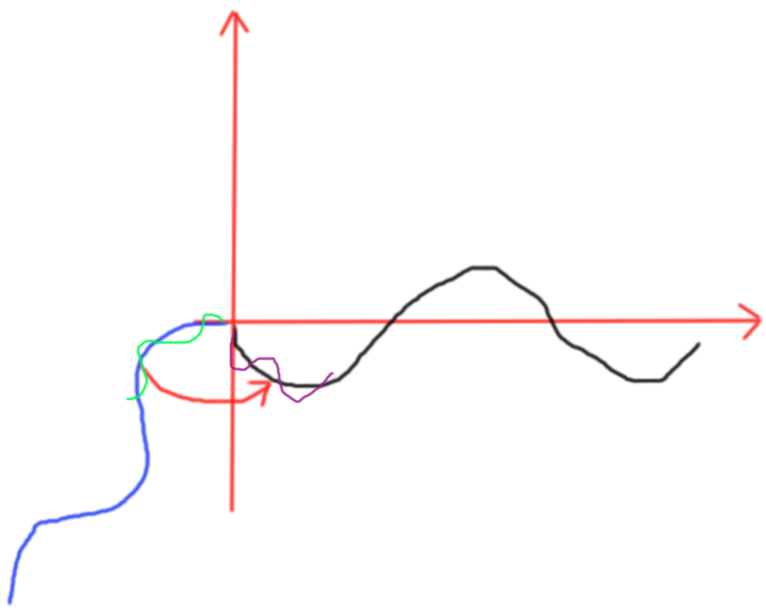

We use P.A.(1.6 GHz) to rotate the ridge-lines and plot them along a horizontal axis.

Rotated ridge-lines with the same P.A.

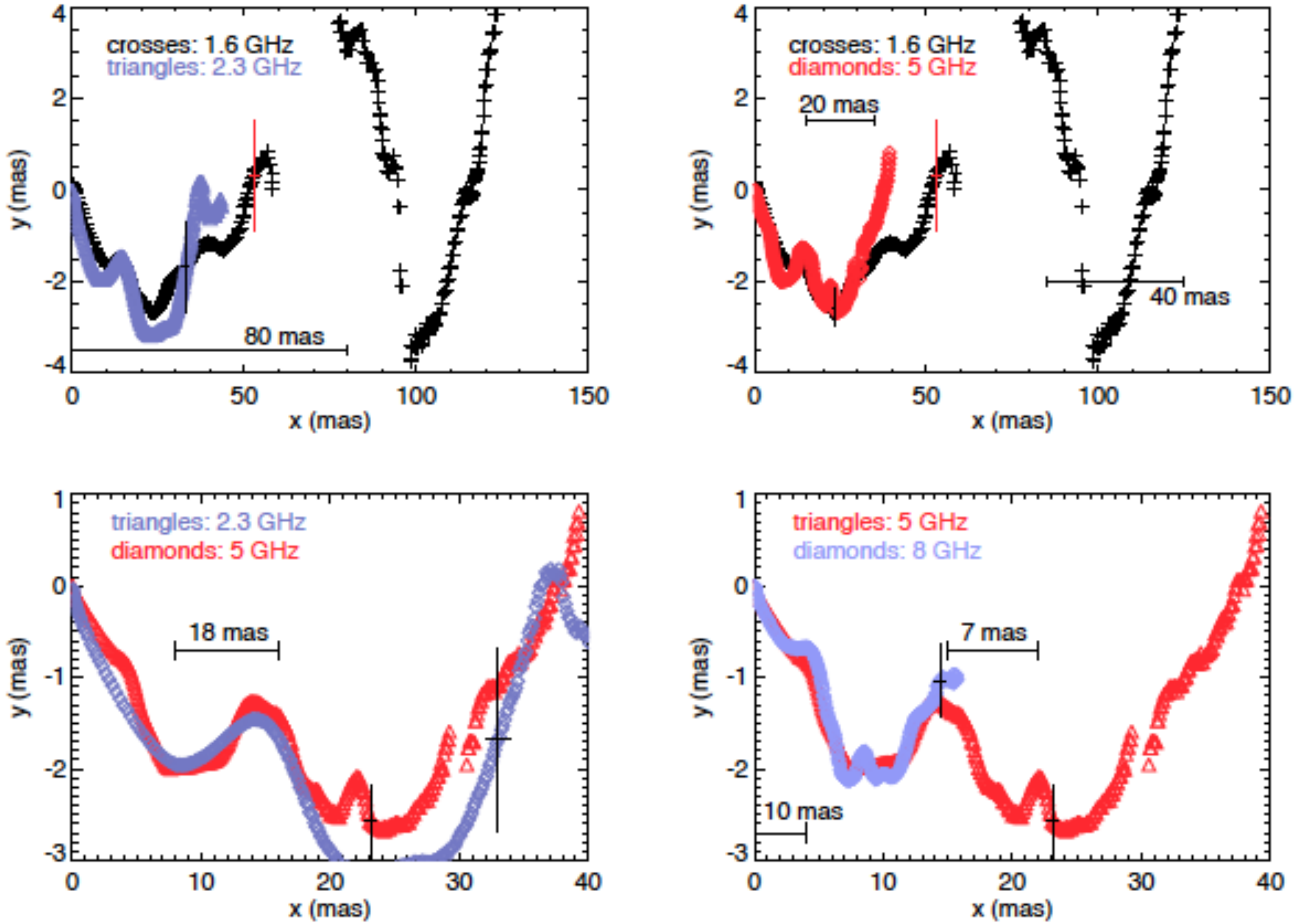

Rotating all ridge-lines with the same angle (1.6 GHz).

Observed opening angles and position angles

Table 2. Observed Jet properties.

	1.6 GHz	5 GHz	8 GHz	15 GHz	22 GHz	43 GHz
Average opening angle	$(12.3 \pm 1.2)^\circ$	$(13.5 \pm 1.3)^\circ$	$(12.1 \pm 0.8)^\circ$	$(10.5 \pm 0.9)^\circ$	18.1°	16.6°
Position angle (χ)	198°	202°	206°	210°	214°	-
Oscillation wavelengths (0-10 mas)	10 - 80	10	10	10	-	-
Oscillation wavelengths (10-35 mas)	20 - 80	20	7-20	20	-	-
Oscillation wavelengths (>35 mas)	40 - 80	-	-	-	-	-

The jets observed at higher frequencies show the direction of propagation of the ridge-line at lower frequencies. In other words, high–frequency jets develop on top of the ridge-line of the jet at low frequency.

The different position angles give a natural explanation to parsec-to-kiloparsec scale misalignment in helical jets.

The opening angles are obtained following the same methodology as given in Pushkarev et al. (2009).

Mean jet opening angle: $12\overset{\circ}{.}1 \pm 0\overset{\circ}{.}8$ At 3º viewing angle: $0\overset{\circ}{.}63 \pm 0\overset{\circ}{.}04$

Rotated ridge-lines from the 15 GHz observations

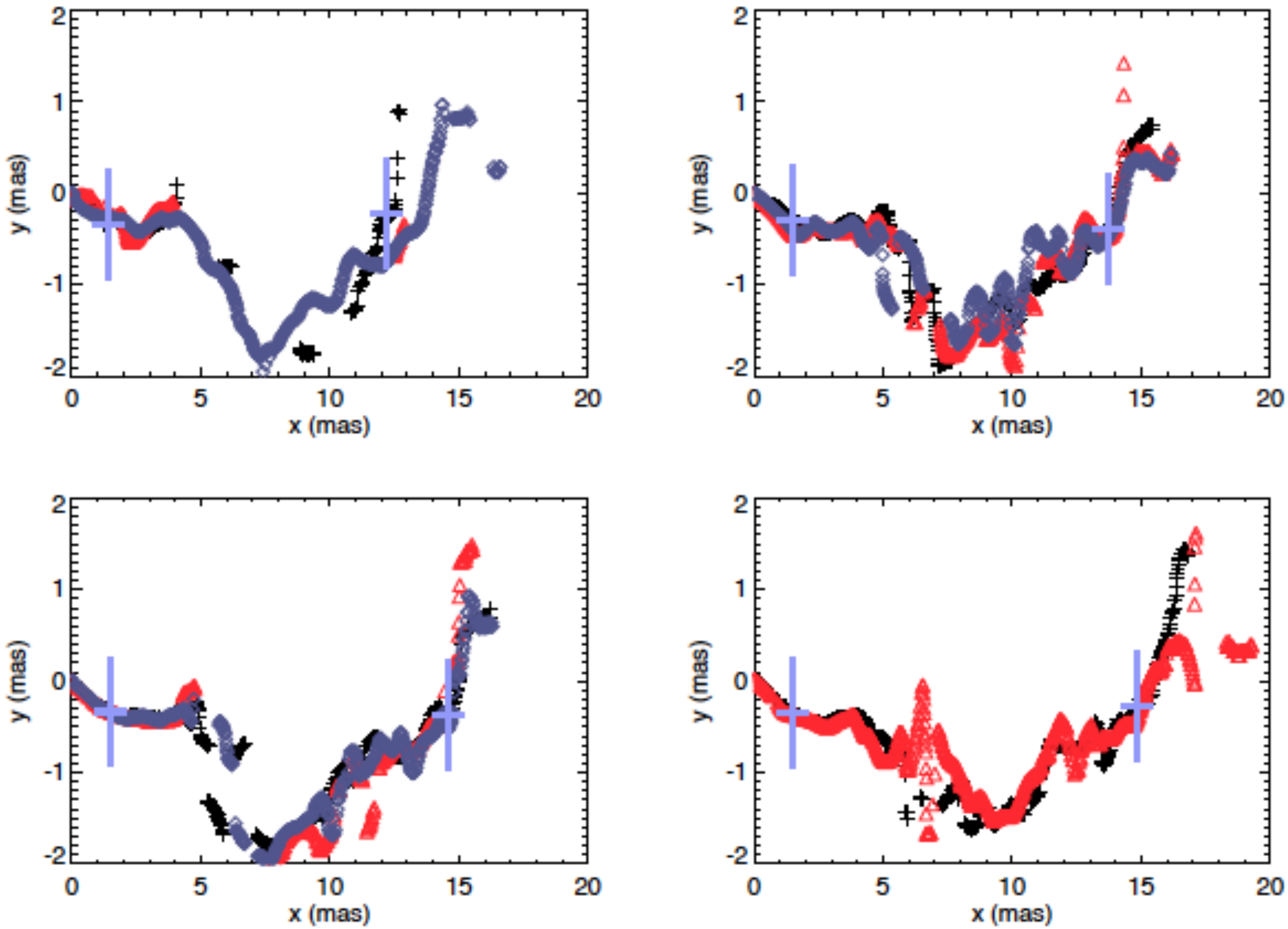

15 GHz at different epochs (MOJAVE data 1998-2009).

Vertical displacements of the 15 GHz ridge-lines

2002 - 2003 | 2008 - 2009

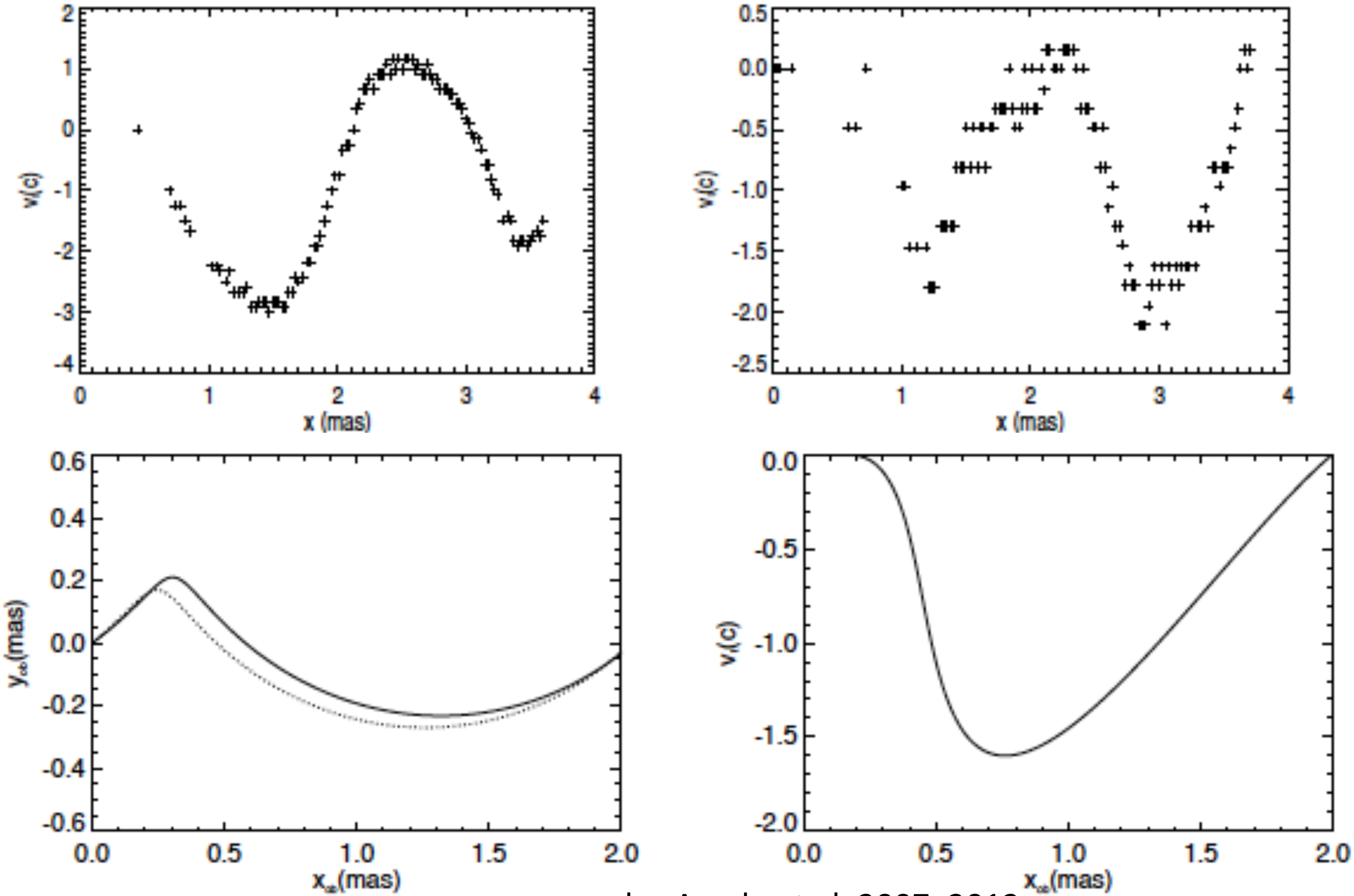

see also Agudo et al. 2007, 2012

Vertical displacements of the 15 GHz ridge-lines

2002 - 2003

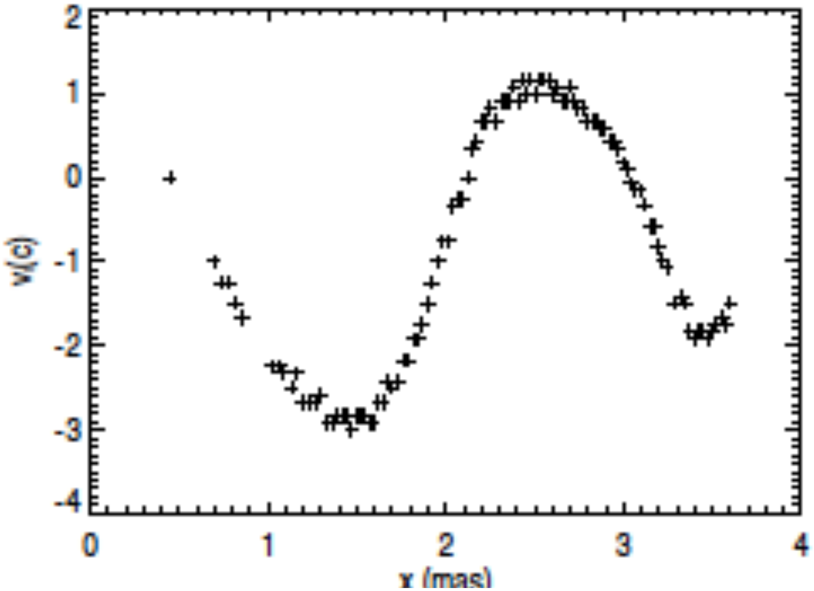

2008 - 2009

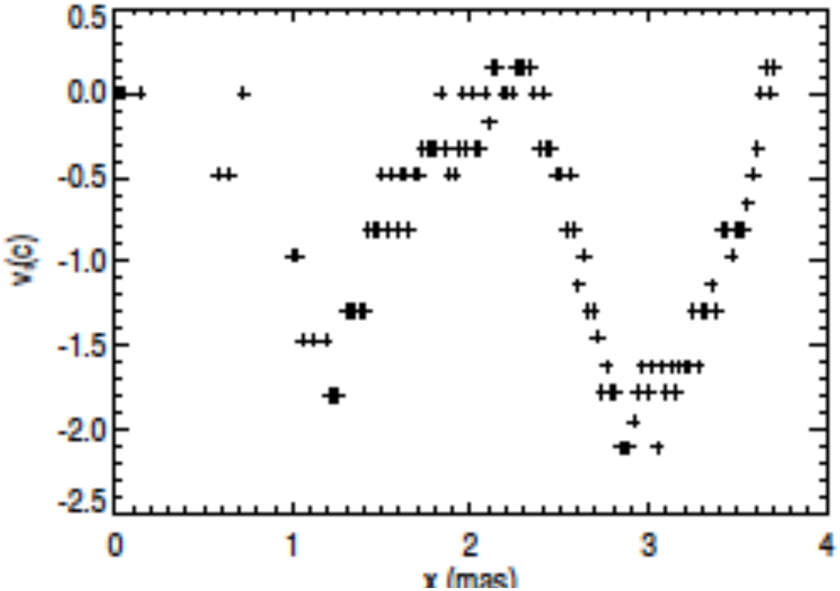

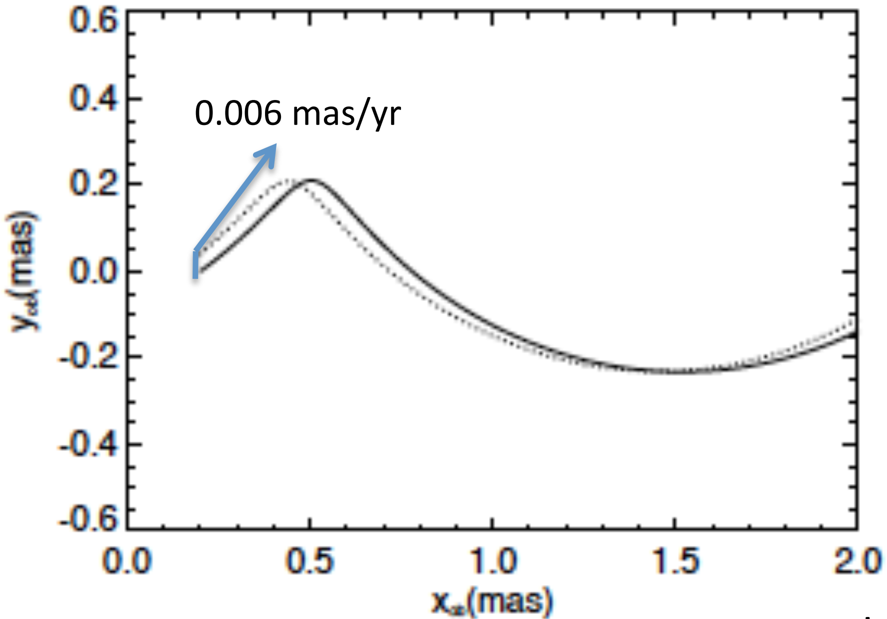

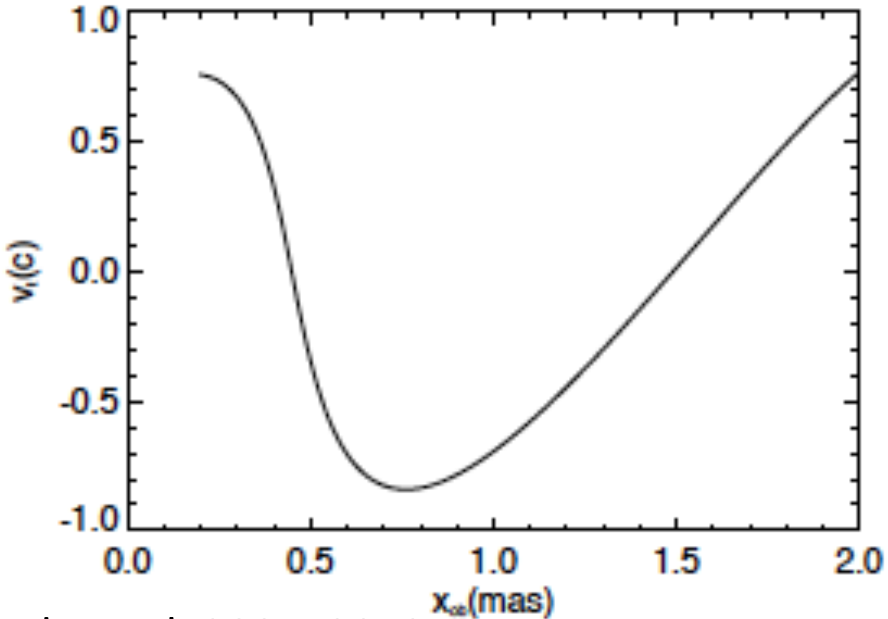

see also Agudo et al. 2007, 2012

An FRII jet disrupted by a helical instability?

A recent observation of this source using EVN and MERLIN confirms this result.
Perucho, Martí-Vidal, Lobanov & Hardee (2012).

VLBI jet

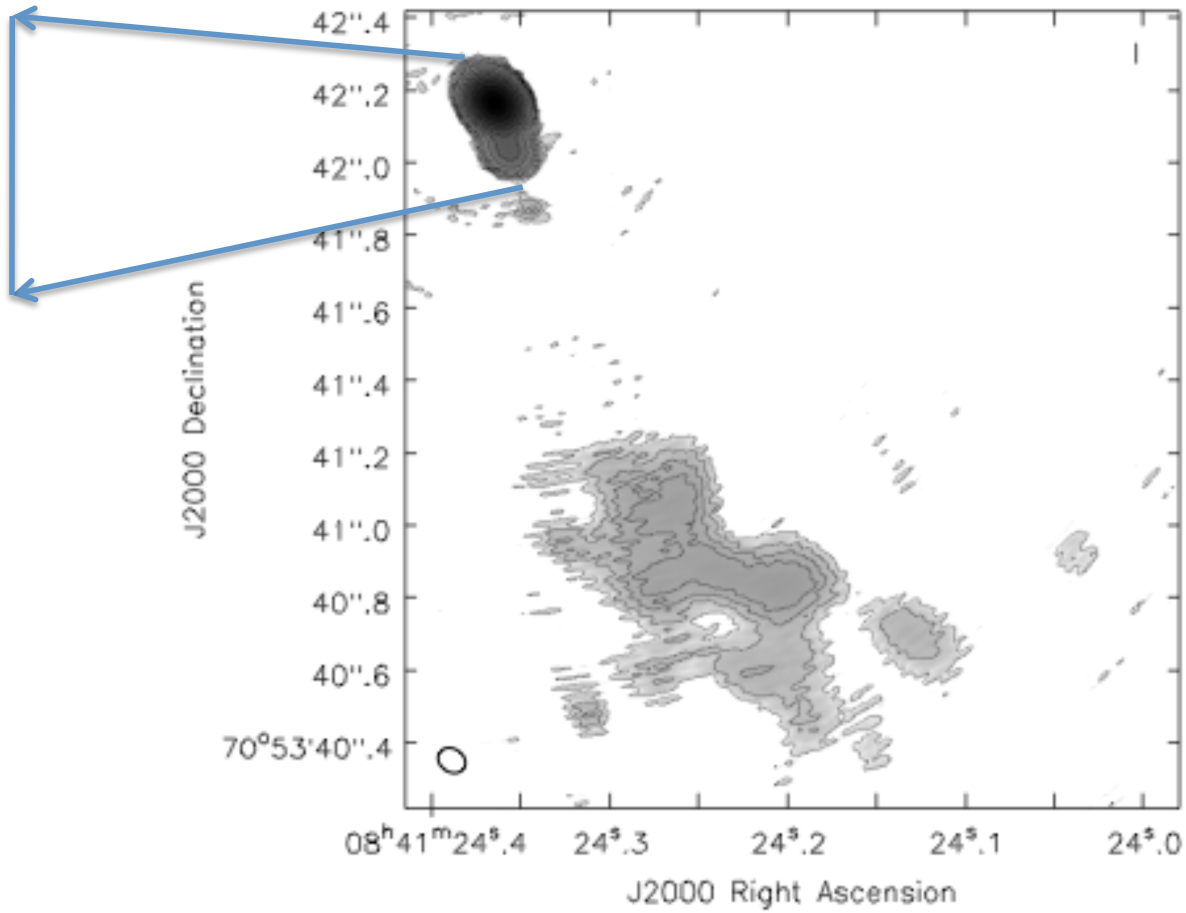

This FRII-classified jet could be disrupted by the growth of an instability, probably Kelvin-Helmholtz.

- The observed growth in amplitude is consistent with estimated growth-rates of unstable modes (Perucho & Lobanov 2007, 2011, Perucho et al. 2012).

Conclusions

- Ridge-lines correspond to physical structures.
- Possible causes:
  - Longer wave: long-term precession at the formation region (10^7 yr periodicity).
  - Shorter waves: shorter period asymmetries at the formation region or downstream.
- When possible to measure, the transversal velocity shows a wave-structure and superluminal values.
  - We observe the motion of a wave pattern, and not the flow itself. The flow moves through the pattern, which most probably corresponds to pressure maxima across the jet cross-section.
  - Small scale transversal core motion plus errors associated to the determination of the ridge-line due to resolution, can explain the superluminal values.

- The source will be observed with Radioastron + global VLBI next year (will allow comparison with VSOP observations).